8-1986

The Abel Inversion of Noisy Data Using Discrete Integral Transforms

Subramania I. Sudharsanan
University of Tennessee - Knoxville

To the Graduate Council:

I am submitting herewith a thesis written by Subramania I. Sudharsanan entitled "The Abel Inversion of Noisy Data Using Discrete Integral Transforms." I have examined the final electronic copy of this thesis for form and content and recommend that it be accepted in partial fulfillment of the requirements for the degree of Master of Science, with a major in Electrical Engineering.

Bruce W. Bomar, Major Professor

We have read this thesis and recommend its acceptance:

Roy Joseph, Dennis Keefer

Accepted for the Council:
Carolyn R. Hodges

Vice Provost and Dean of the Graduate School

(Original signatures are on file with official student records.)

To the Graduate Council:

I am submitting herewith a thesis written by Subramania I. Sudharsanan entitled "The Abel inversion of Noisy Data Using Discrete Integral Transforms." I have examined the final copy of this thesis for form and content and recommend that it be accepted in partial fulfillment of the requirements for the degree of Master of Science, with a major in Electrical Engineering.

Bruce W. Bomar, Major Professor

We have read this thesis
and recommend its acceptance:

Accepted for the council:

Vice Provost
and Dean of The Graduate School

STATEMENT OF PERMISSION TO USE

In presenting this thesis in partial fulfillment of the requirements for a Master's degree at The University of Tennessee, Knoxville, I agree that the Library shall make it available to borrowers under rules of the Library. Brief quotations from this thesis are allowable without special permission, provided that accurate acknowledgment of the source is made.

Permission for extensive quotation from or reproduction of this thesis may be granted by my major professor, or in his absence, by the Head of Interlibrary Services when, in the opinion of either, the proposed use of the material is for scholarly purposes. Any copying or use of the material in this thesis for financial gain shall not be allowed without my written permission.

Signature S. Sudharsanan

Date 08/08/1986

THE ABEL INVERSION OF NOISY DATA USING DISCRETE INTEGRAL TRANSFORMS

A Thesis

Presented for the

Master of Science

Degree

The University of Tennessee, Knoxville

Subramania I. Sudharsanan

August 1986

ACKNOWLEDGMENTS

The Author would like to express his appreciation to Dr. Bruce Bomar, who served as the chairman of the committee and Dr. Roy Joseph who served as a member, for their helpful advice and guidance.

Special thanks are due to Dr. Dennis Keefer and Mr. Montgomery Smith for their consistent encouragement, and invaluable support and guidance in conducting this investigation and preparing the manuscript. The thesis would not be realized without their help.

Thanks are extended to Mr. Richard Welle for numerous helps in performing the data analysis.

ABSTRACT

The determination of a radially symmetric two-dimensional function from its one dimensional projection is known as Abel inversion. This finds applications in several fields of engineering and science including astronomy, image processing, plasma diagnostics and optics. One radial slice of the function, which completely specifies the two-dimensional function, is the inverse Hankel transform of the Fourier Transform of the projection. With the projection data available as a discrete signal, the Abel inversion can be performed using the discrete Fourier transform and the inverse Hankel transform. The existing techniques to compute inverse Hankel transforms are discussed and a modification to one of those methods is introduced and shown to yield reasonably accurate results with significantly fewer calculations. The efficient fast Fourier transform is used in the evaluation of both the transforms.

Experimentally obtained projection data, which is usually noisy and off-center, is dealt with in the Fourier domain using a frequency domain filter and a maximum likelihood estimator derived from the assumed noise characteristics. The maximum likelihood estimator is used to estimate the Fourier transform of the properly centered data. Results of numerical experiments are given to verify the method. The proposed method is computationally more efficient than the existing curve-fitting methods for performing the Abel inversion of noisy data.

TABLE OF CONTENTS

LIST OF FIGURES

CHAPTER I

INTRODUCTION

The reconstruction of a circularly symmetric two-dimensional function from a projection onto its radial axis is known as Abel inversion or inverse Abel transformation of the projection. Applications of the Abel inversion are found in numerous fields including astronomy, image processing, optics and plasma diagnostics[1,2]. One important application is the determination of the radial distribution of emission coefficients from the experimentally obtained radiant intensity of a circularly symmetric plasma. This problem arises when determining the thermodynamic properties of high temperature plasmas of optically thin and axisymmetric configurations. The measured intensity, $I(x)$, is given in terms of emission coefficients, $\epsilon(r)$, through the Abel transform [1]*

$$I(x) = 2 \int_{x}^{\infty} \frac{r\epsilon(r)dr}{\sqrt{r^2 - x^2}} \tag{1.1}$$

where x is the displacement of the intensity profile and r is the radial distance of the source (Figure 1.1). $I(x)$ is the one-dimensional projection of the two-dimensional circularly symmetric function having $\epsilon(r)$ as a radial slice. Figure 1.1 shows the geometry of the cross-section of an axisymmetric plasma of

* Numbers in brackets refer to similarly numbered references in the Bibliography.

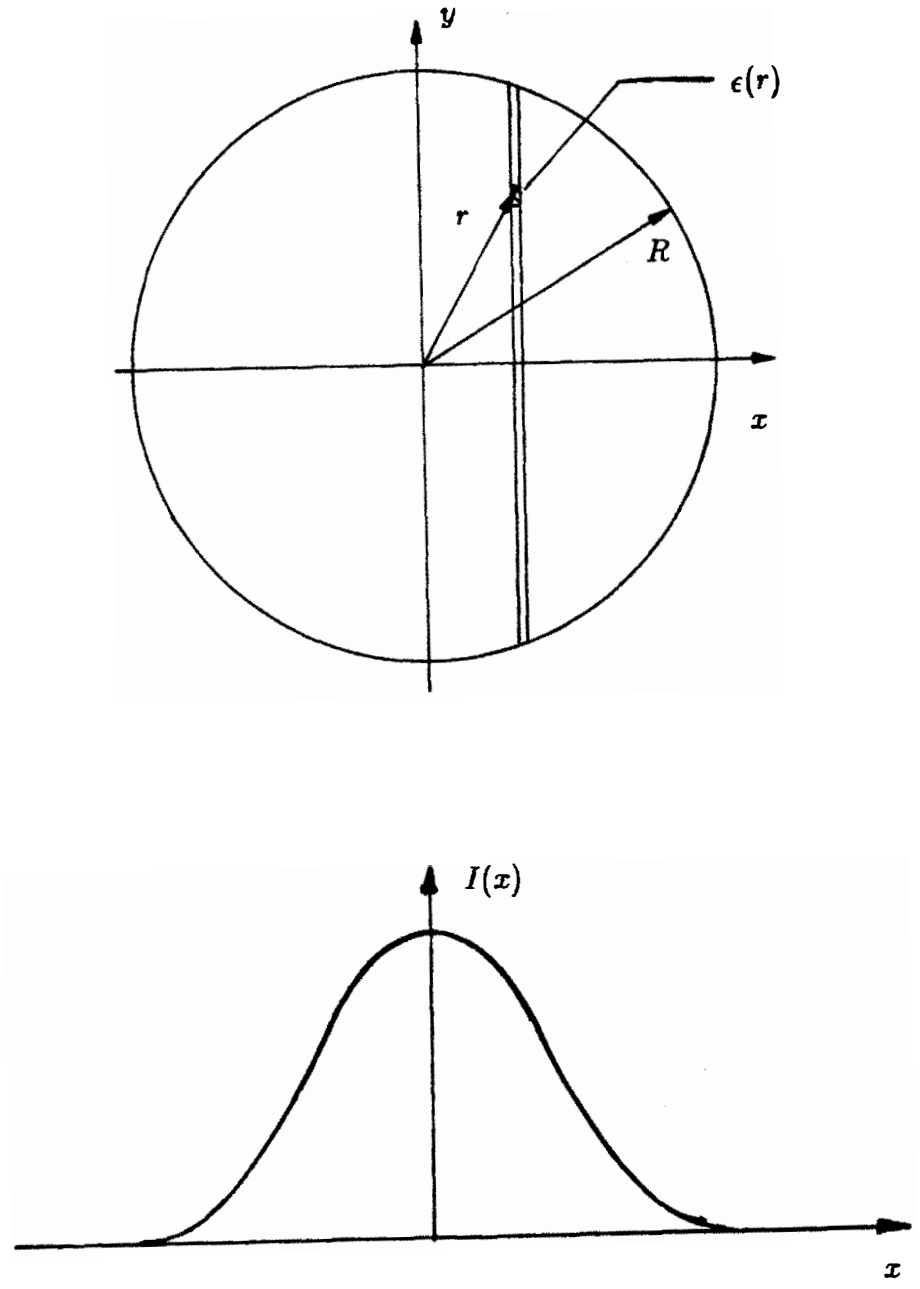

Figure 1.1. The cross-section and intensity profile of an axisymmetric plasma.

overall radius R. The inversion integral, that is the inverse Abel transform is given by,

$$\epsilon(r) = \frac{-1}{\pi} \int_{r}^{\infty} \frac{(dI/dx)}{\sqrt{x^2 - r^2}} dx \tag{1.2}$$

which can be used to calculate the temperature of the plasma. The problem is to evaluate the integral in Equation 1.2.

In most practical applications the intensity is not available as a continuous function and is known only at discrete sample points. Also, the intensity data is found to be corrupted by noise. Several methods ranging from geometrical techniques to numerical methods using polynomial fits have been used to perform the inversion. Nestor and Olsen [3] transformed the variables according to $r^2 = v$ and $x^2 = u$ so that the inversion integral can be approximated by a simpler sum. Bockasten [4] fitted third degree polynomials to the data points and approximated the integral by a sum. However these methods require prior smoothing of the data and are not considered complete in themselves.

Later, the least squares curve fit methods were suggested and proved to yield better results than the exact fit methods due to the noise in the intensity data. Freeman and Katz [5] approached the problem by a single curve fit to the data. Fourth order polynomials were found to give the best results among the trials using up to twelfth order polynomials. Cremers and Birkebak [6] compared several inversion techniques and showed that the least squares curve fitting

techniques are more favorable than the exact fit methods. Short descriptions of several other techniques and comparison of the above mentioned techniques can also be found in [6]. Shelby [7] divided the data into several intervals and used a least squares polynomial fit technique in each interval to smooth the scattered data. The inversion was then performed analytically and summed over the intervals to obtain emission coefficients. Maldonado *et al.* [8] expanded $\epsilon(r)$ in a series of orthogonal polynomials and derived a method to find the expansion coefficients from the intensity data.

All the above mentioned methods have several drawbacks. These methods had to treat the singularity in the lower limit of the integral. Handling the singularity posed problems in the numerical or analytical schemes. The smoothing techniques used are effectively a kind of lowpass filtering. When the inversion is performed, the spectral characteristics of the noise, of the desired signal and of the smoothing algorithm are not considered. That is, the possible problems of loss of information and distortion are neglected. Also, the inversion assumes symmetry of input data. The measured intensity data is usually symmetric about some unknown point, but not about zero of the x axis. That is, the data is shifted or off-center. (Throughout this report, unless otherwise mentioned, the word symmetry stands for symmetry about the origin or zero of the independent continuous variable.) With the existing techniques symmetrizing has to be performed by trial and error approach in the least squares

sense. This approach does not allow the best symmetric sampling point to have a non-integer shift from the geometrical center for a particular set of data. The smoothing techniques consume a large amount of computer time and the error propagation calculations are tedious [7].

The technique described in this report greatly differs from curve-fitting techniques in its use of integral transforms. In Chapter II the inverse Abel transform for a function is shown to be equivalent to the Fourier transform followed by the inverse Hankel transform. There are several well known techniques for performing the Fourier transform. Computation of inverse Hankel transform, which is used in many other areas of science and engineering is also discussed in Chapter II.

In Chapter III, the techniques to handle actual data are presented. Reduction of noise is conveniently handled in the Fourier domain using well known digital filters. The best symmetric point is found using an algorithm which uses a maximum likelihood estimator derived from the possible noise characteristics and certain of the Fourier transform. Numerical experiments are carried out in Chapter IV to demonstrate the validity and applicability of the method.

CHAPTER II

NUMERICAL IMPLEMENTATION

Theoretical Background

As stated in Chapter I, the inversion technique described in this chapter uses integral transforms. Before the integral transforms are discretized to compute the inversion numerically , it is necessary to see how the Abel inversion is related to certain integral transforms. The following derivation has appeared in published papers and is a special case of signal reconstruction from projections used in image processing and computed tomography [9].

First, rewrite Equation 1.1 using $r = \sqrt{x^2 + y^2}$ and changing the integration variable to y so that $dr = ydy/\sqrt{x^2 + y^2} = ydy/r$,

$$I(x) = 2 \int_0^\infty \epsilon(\sqrt{x^2 + y^2}) dy$$

$$I(x) = \int_{-\infty}^{\infty} \epsilon(\sqrt{x^2 + y^2}) dy \quad . \tag{2.1}$$

The Fourier transform of $I(x)$ is

$$FT[I(x)] = \int_{-\infty}^{\infty} I(x) e^{-j2\pi\rho x} dx \quad . \tag{2.2}$$

Using Equation 2.1 and changing to polar coordinates,

$$FT[I(x)] = \int_0^{\infty} \int_0^{2\pi} \epsilon(r) e^{-j2\pi\rho r\cos\theta} r d\theta dr \tag{2.3}$$

$$FT[I(x)] = \int_0^{\infty} r\epsilon(r) 2\pi [\frac{1}{2\pi} \int_0^{2\pi} e^{-j2\pi r\rho\cos\theta} d\theta] dr \quad . \tag{2.4}$$

The integral in the brackets is known as the zero-order Bessel function [10], $J_0(2\pi r\rho)$. Thus,

$$FT[I(x)] = 2\pi \int_0^{\infty} r\epsilon(r) J_0(2\pi r\rho) dr \quad . \tag{2.5}$$

The right hand side of this equation is known as the zero-order Fourier-Bessel or zero-order Hankel transform of $\epsilon(r)$ [2].

Hence,

$$FT[I(x)] = HT[\epsilon(r)] \tag{2.6}$$

$$\epsilon(r) = HT^{-1}[FT[I(x)]] \quad . \tag{2.7}$$

Therefore, $\epsilon(r)$ can be obtained from $I(x)$ by means of Fourier and inverse Hankel transforms. The procedure can be written analytically in two steps as follows:

$$G(f) = \int_{-\infty}^{\infty} I(x) e^{-j2\pi f x} dx \tag{2.8}$$

$$\epsilon(r) = 2\pi \int_{0}^{\infty} G(f) f J_0(2\pi f r) df \quad . \tag{2.9}$$

Note that the inverse Hankel transform is same as the forward transform [2].

Numerical Procedure

As mentioned earlier, the intensity data, $I(x)$, is available only at discrete sample points. It can be written as a sequence, $I(i\Delta x)$; $i = 0, 1, ..., N-1$, for N sample points with a uniform spacing of Δx. Approximating the Fourier integral in Equation 2.8 by a summation gives

$$G(f) \approx \sum_{i=0}^{N-1} I(i\Delta x) e^{-j2\pi \Delta x f} \Delta x \quad . \tag{2.10}$$

Computing $G(f)$ at discrete frequency points $\Delta f k$; $k = 0, 1, ..., N-1$, such that $\Delta x \Delta f = 1/N$ then gives

$$G(k\Delta f) \approx \sum_{i=0}^{N-1} \hat{I}(i) e^{-\frac{2\pi i k}{N}} = \hat{G}(k) \tag{2.11}$$

where the sequence $\hat{I}(i) = I(i\Delta x)\Delta x$. Equation 2.11 is the discrete Fourier transform (DFT) of the intensity samples. The reader is referred to [11] and [12]

to see a complete discussion on DFT, including the periodic nature of DFT, the effect of under sampling and the relationship with the Fourier transform.

The principal advantage of using the DFT is the existence of fast algorithms to compute the DFT. The algorithms are generally classified as fast Fourier transform (FFT) algorithms. While a direct evaluation of the DFT requires in the order of N^2 complex additions and multiplications, the FFT requires in the order of $(N/2)log_2 N$ complex operations [12]. Note that N must be an even integer which can be written as a power of two. Several FFT algorithms have been proposed and implemented both in the form of hardware and software. In this report the algorithm known as the Radix-2 FFT method is used to compute the DFT.

Note that since $\hat{I}(i)$ is a real and symmetric (even) sequence, so is the DFT $\hat{G}(k)$ [12]. Thus, it is now required to perform the Hankel transform operation on the obtained real sequence $\hat{G}(k)$. Due to symmetry, only $N/2$ points of the DFT will be required.

The computation of the Hankel transform or its inverse is of interest in a wide variety of disciplines in engineering and physics. Several interesting methods have been proposed to perform the Hankel transform efficiently and accurately. The importance of those methods can be appreciated once we try to perform the transform in a direct manner.

If the sampling in x, f and r is such that $x = \Delta x i$, $f = \Delta f k$ and $r = \Delta r l$

then the integral $2\pi \int_0^\infty G(f) f J_0(2\pi r f) df$ can be approximated by a sum as

$$\epsilon(\Delta r l) = 2\pi \sum_{k=0}^{N/2-1} G(\Delta f k) \Delta f k J_0(2\pi \Delta r l \Delta f k) \Delta f \quad . \tag{2.12}$$

With $\Delta x \Delta f = 1/N$ and $\Delta f \Delta r = 1/N$ (i.e. $\Delta r = \Delta x$), Equation 2.12 becomes

$$\hat{\epsilon}(l) = \frac{2\pi}{N^2(\Delta x)^2} \sum_{k=0}^{N/2-1} \hat{G}(k) k J_0(\frac{2\pi l k}{N}) \tag{2.13}$$

where $\hat{\epsilon}(l) = \epsilon(\Delta r l)$ and $\hat{G}(k) = G(\Delta f k)$.

It is easily seen that the evaluation of the Hankel transform by direct discretization involves calculation of zero-order Bessel functions for various arguments. The Bessel functions can be calculated using polynomial approximations given by Abramovitz and Stegun [10]. If several sets of data are to be processed the Bessel functions can be calculated and stored in a look-up table. However, about M^2 multiplications and M^2 additions are still required for an M-point Hankel transform routine.

The early methods proposed by Brunol and Chavel [13] and Oppenheim *et al.* [14] require arithmetic operations in the order of M^2 along with extensive storage requirements or numerous function evaluations. However, the method proposed in [14] uses the projection slice theorem and is the basis for recently proposed faster techniques.

Siegman [15], who presented the first quasi-fast algorithm, changed the

variable within the integral to obtain the form of a convolution integral that can be evaluated using efficient FFT's. The variables are transformed into $f = f_0 e^{\alpha u}$ and $r = r_0 e^{\alpha v}$. It is easily seen that the method requires exponential sampling of the input and output and also certain end correction term may be required to obtain an accurate result [15].

Another approach, proposed by Mook [16], uses a square-root grid sampling of the input to compute the Abel transform by a convolution integral followed by an FFT to obtain Hankel transform. The methods described by Siegman and Mook can not be used for our application because of the non-uniform sampling requirements.

Another method proposed by Murphy and Gallager [17] uses two-dimensional FFT's to compute the Hankel transform. If the input is a circularly symmetric two-dimensional function with one radial slice being $G(f)$, then the input matrix can be partitioned into smaller processing blocks by two-dimensional extension of the one-dimensional FFT butterflies. However this method is also not suitable for our application due to the two-dimensional requirements on input and output. Another common procedure is to expand the Bessel functions asymptotically in terms of trigonometric functions and to exploit the efficiency of the FFT [14,17], the solutions however are only asymptotic. That is, the solution will not be correct for smaller arguments, but for larger arguments.

A novel technique for performing the Hankel transform, known as Fourier

selection summation (FSS) algorithm, has been proposed by Candel [18]. The FSS algorithm uses a $2M$-point FFT followed by M^2 additions to perform an M-point Hankel transform routine. Candel's algorithm uses uniform sampling and is both accurate and relatively fast. A description of the FSS algorithm is given here followed by a modification to the algorithm to increase the speed at the expense of accuracy.

The function $G(f)$ is not defined on the negative f axis (see Equation 2.9). If $G(-f) = -G(f)$ then the function $fG(f)$ will be an even function. This allows the integral in Equation 2.9 to be expressed as

$$\epsilon(r) = \pi \int_{-\infty}^{\infty} fG(f)J_0(2\pi rf)df \quad . \tag{2.14}$$

The zero-order Bessel function can be expressed by a finite integral [19] as

$$J_0(\alpha) = \frac{1}{\pi}\int_{-1}^{+1} \frac{e^{-j\alpha t}}{\sqrt{1-t^2}}dt \quad . \tag{2.15}$$

With this representation,

$$\epsilon(r) = \int_{-\infty}^{\infty} fG(f) \int_{-1}^{+1} \frac{e^{-j2\pi frt}}{\sqrt{1-t^2}}dtdf \quad . \tag{2.16}$$

Substituting $t = \cos\theta$ (t varies from -1 to +1) and interchanging the order of integration results in

$$\epsilon(r) = \int_0^{\pi} \int_{-\infty}^{\infty} fG(f) e^{-j2\pi f r \cos\theta} df\, d\theta \quad . \tag{2.17}$$

If the Fourier transform of $fG(f)$ is $\phi(\varsigma)$, then the Equation 2.17 can be written as

$$\epsilon(r) = 2 \int_0^{\pi/2} \phi(r\cos\theta) d\theta \tag{2.18}$$

where the symmetry in ς domain makes it possible to change the the integration limits from 0 to π to 0 to $\pi/2$.

It is required to perform the Fourier transform of $fG(f)$ and the integration in Equation 2.18. To obtain an M-point Hankel transform ($M = N/2$), the first step can be performed by a $2M$-point real FFT on $k\hat{G}(k)$,

$$\hat{\phi}(m) = \sum_{k=0}^{N-1} \hat{G}(k) k e^{\frac{-j2\pi km}{N}} \quad ; \quad m = 0, 1, ..., N \quad . \tag{2.19}$$

Note that the function $fG(f)$ is an even function and the discrete sample values for $k = N/2 + 1$ to N correspond to the negative values of f. That is, $(N-k)\hat{G}(N-k) = k\hat{G}(k)$; $k = 0, 1, ..., N/2$. Also,

$$\phi(m\Delta\varsigma) = \hat{\phi}(m)(\Delta f)^2 \tag{2.20}$$

where $\Delta\varsigma$ is the sampling interval in the ς domain. Then the integral in Equation 2.18 can be approximated by a rectangular rule integration

$$\epsilon(r) = 2 \sum_{n=0}^{S/2-1} \phi(r\cos\theta_n)\Delta\theta \tag{2.21}$$

where the integration interval is divided into $S/2$ small intervals of $\Delta\theta$ each so that $\theta_n = \pi n/S$ and $\Delta\theta = \pi/S$. Usually, $S = 2M = N$. Because $\phi(\varsigma)$ is known only at integer sample points, the evaluation of the sum given by Equation 2.21 involves an interpolation problem. A simple efficient procedure is nearest neighbor interpolation. That is, for a particular r the $r\cos\theta_n$ values are approximated to its nearest integer values. The procedure can be given by Equations 2.22 and 2.23. A geometrical representation is shown in Figure 2.1 for the case of $S = M = N/2 = 16$ and $l = 8$ where

$$d(n,l) = l\cos(\theta_n) + 0.5 \quad ; \quad n = 0, 1, ..., S/2 - 1 \tag{2.22}$$

$$\hat{\epsilon}(l) = \frac{2\pi}{S} \sum_{n=0}^{S/2} \hat{\phi}(\text{int}[d(n,l)])(\Delta f)^2 \quad ; \quad l = 0, 1, ..., M - 1 \tag{2.23}$$

and where int[.] represents the integer operation.

Although a linear interpolation approach to evaluate the integral in Equation 2.18 may give more accurate results, examples are presented in Chapter IV that show the overall mean square error in the Abel inversion computed with a Direct Hankel transform routine and the FSS method are quite close and

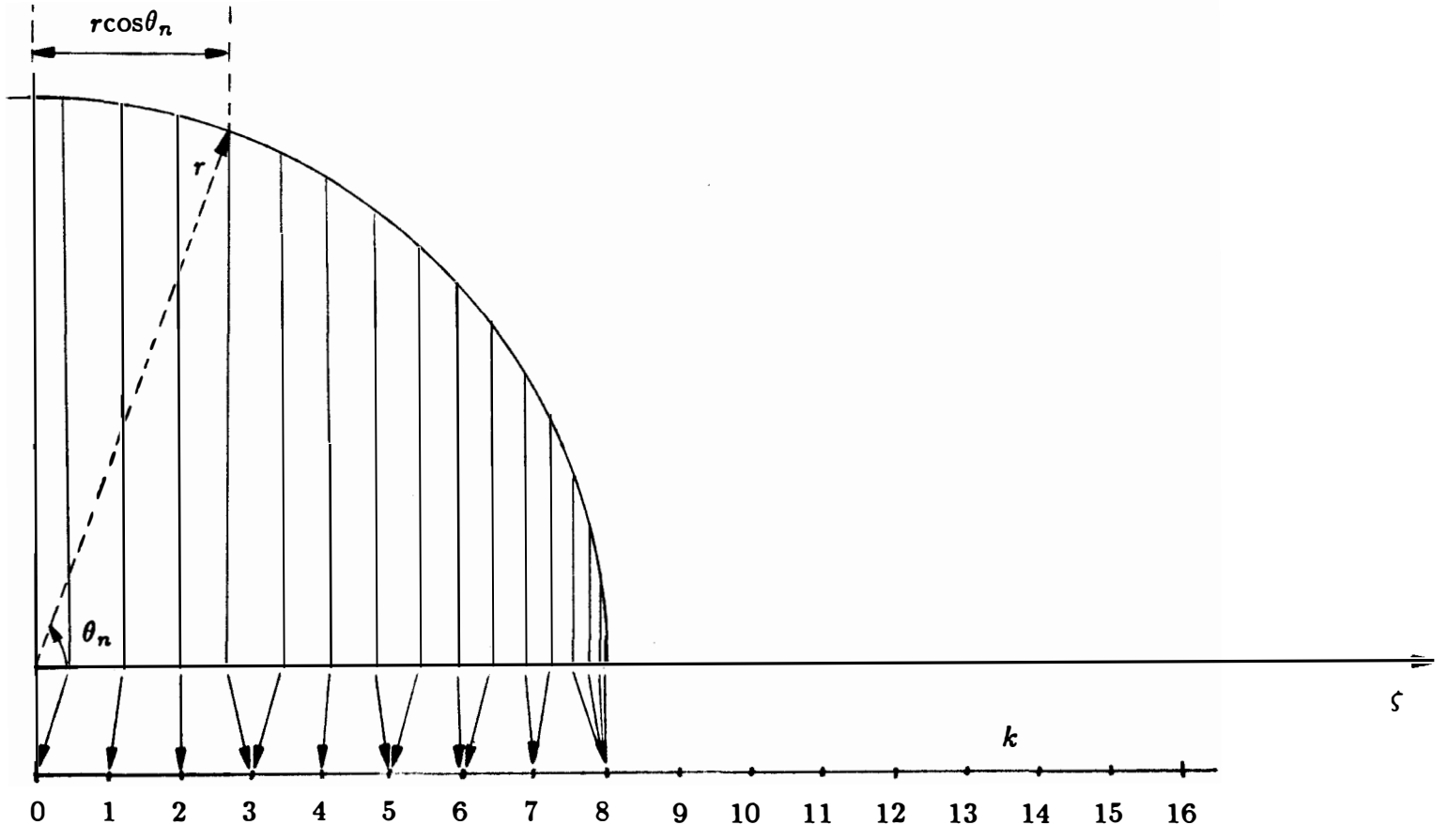

Figure 2.1. Geometric representation of the nearest neighbor interpolation.

within acceptable accuracy limits. The integer values representing $r\cos\theta_n$ can be precomputed and stored in a look-up table to increase computational efficiency, particularly when several sets of data are processed. So the number of arithmetic operations to compute an M-point Hankel transform will then be equivalent to a $2M$-point real FFT plus $2M$ multiplications and M^2 additions.

Although this technique is faster than the Direct method, it still can not be considered as a fast Hankel transform algorithm because it requires M^2 additions. This large number of additions occurs when evaluating the integral in Equation 2.18. Each Hankel transform estimate, $\hat{\epsilon}(l)$, requires $M = S/2$ additions to calculate that integral using l Fourier components, $\hat{\phi}(k)$; $k = 0, 1, ..., l$. One possible way of reducing the number of additions is to set $S = 2l$ so that each Hankel transform estimate, $\hat{\epsilon}(l)$, requires l additions to compute the integral using l Fourier components. The procedure can be given by Equations 2.24 and 2.25 where

$$d(n,l) = l\cos(\theta_n) + 0.5 \;\; ; \;\; n = 0, 1, ..., l \tag{2.24}$$

$$\hat{\epsilon}(l) = \frac{\pi}{l} \sum_{n=0}^{l} \hat{\phi}(\text{int}[d(n,l)])(\Delta f)^2 \;\; ; \;\; l = 0, 1, ..., M-1 \quad . \tag{2.25}$$

If the integer values of $d(n,l)$ are stored in a look-up table, the number of additions required to calculate the integral will be $M^2/2$. Also, the storage

requirements will be reduced to $M^2/2$. This approach will be referred to as modified Fourier selection summation (MFSS) algorithm.

In the MFSS method the integration step size, $\Delta\theta$, gradually decreases from lower order estimates to the higher order ones. Hence, it may be expected that the lower order components are less accurate than the estimates obtained by the FSS technique. However, the nearest neighbor interpolation is used in both the FSS and the MFSS method and the accuracy can not solely be determined by the integration step size. In Chapter IV experiments comparing the Direct, the FSS and the MFSS approaches are carried out.

Another technique, again proposed by Candel [20], uses the FSS algorithm and the asymptotic expansion of the Bessel function. The asymptotic expansion of the zero-order Bessel function in terms of trigonometric functions can be found in Abramovitz and Stegun [9]. This allows the computation of higher order components of the Hankel transform by the FFT. To obtain higher accuracy, more trigonometric functions can be included in the asymptotic expansion, which will result in more FFT's. However, the lower order components are still computed by the FSS algorithm and because of this the method is called the Dual algorithm. The transition from the FSS estimation to asymptotic evaluation can occur at some $l = L$ where an acceptable error criterion is satisfied. Candel gives an empirical value for L at which the asymptotic Hankel transform will converge to the exact transform within a small amount of error. With the first order

asymptotic expansion, which requires one $2M$-point FFT, the usual values for L are around 25. It is suggested that a second order approximation, which requires two $2M$-point FFT's, compares better over the first order approximation and the value for L is also slightly greater than 10 for well behaved functions. Tables 2.1 and 2.2 show that up to $M = 256$ the MFSS method compares better in terms of arithmetic operations over the Dual algorithm with a second order asymptotic approximation. In our practical application of the Abel inversion, a 128-point Hankel transform need be performed so it can be performed with less computational efforts by the MFSS technique.

Table 2.1. Computational complexity for an M-point Hankel transform.

Method	Multiplications	Additions
Direct	M^2	M^2
FSS	$6M + 2Mlog_2M$	$10M + 3Mlog_2M + M^2$
MFSS	$6M + 2Mlog_2M$	$10M + 3Mlog_2M + M^2/2$
Dual	$18M + 8Mlog_2(2M)$	$14M + 12Mlog_2(2M) + 3Mlog_2M + LM$

Table 2.2. Computational complexity for 128 and 256 point Hankel transforms (L=12).

		Direct	FSS	MFSS	Dual
$M = 128$	Multiplications	16384	2560	2560	10496
	Additions	16384	20352	12160	18304
$M = 256$	Multiplications	65536	5632	5632	23040
	Additions	65536	74240	41472	40448

CHAPTER III

INVERSION OF NOISY DATA

In the application of determining the thermodynamic properties of plasma, the radiant intensity is imaged, digitized and stored in as a 512 by 240 array of 16-bit integers. A dedicated digital image processor is used to handle these digitized images where each column in the array corresponds to one set of intensity data [21]. Figure 3.1 shows a typical measured intensity profile from a laser sustained argon plasma. The data clearly is corrupted with noise and off-center. For the technique described in Chapter II the input data must be symmetric and it is not known how the algorithm behaves for noisy data. The reduction of noise may be handled by a properly designed frequency domain filter. It is also necessary to determine the point about which the data is symmetric since the input data is required to be symmetric about origin.

A frequency domain filter can easily be justified and conveniently implemented since the inversion is performed through Fourier domain. To design the filter the input noise has to be modeled and also the resulting output characteristics for that model have to be predicted. A detailed study of the effects of input noise in the Abel inversion is given by Smith [22]. In [22], the input noise is assumed to be a zero mean, wide sense stationary, bandlimited white noise; this assumption is justified for the measured plasma intensity data.

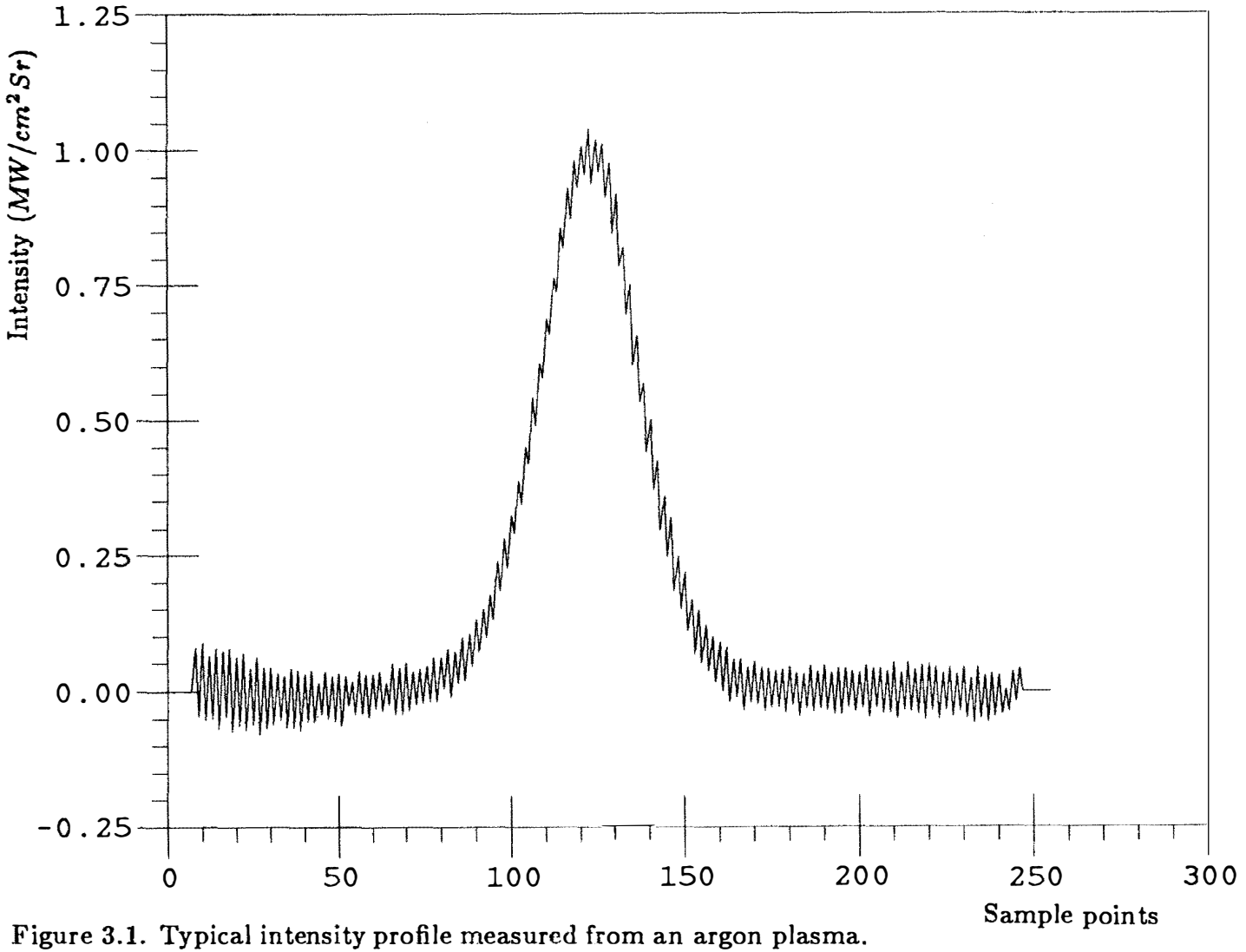

Figure 3.1. Typical intensity profile measured from an argon plasma.

The output noise characteristics are shown to be nonstationary and the variance of the output noise is shown to be proportional to the cube of the bandwidth and inversely proportional to the radial displacement r. A lowpass filter having as narrow a passband bandwidth as possible is desired since the output noise variance depends on the cube of the bandwidth. In general the input function has most of its energy in the low frequency range so the bandwidth can be small. However, the filtering should not introduce distortion of the desired signal. Therefore, the selection of the passband edge frequency for the lowpass filter to be used will depend on the input function's frequency characteristics. In Chapter IV numerical examples are used to determine how to select the passband edge frequencies.

Once the filter passband edge frequency is determined for the filter, we still have choices on the kind of filter to be used. A simple lowpass Butterworth filter is suggested by Gonzalez [23]. The filter transfer function is multiplied by the DFT of the input, where the DFT is obtained without zero-padding the input. Note that zero-padding the input is usually carried out to avoid circular convolution when the convolution is performed by DFT's. This Butterworth filter is very useful when the spectrum of the desired signal falls off rapidly and when most of its energy is within the passband. The experiments in Chapter IV show that this filter is useful for Gaussian type input functions and does not present any circular convolution problems. The N^{th} order Butterworth filter

transfer function proposed by Gonzalez is given by [23],

$$H(f) = \frac{1}{1 + \left(\frac{f}{f_c}\right)^{2N}} \quad . \tag{3.1}$$

The passband bandwidth is varied by varying f_c. The frequency response of a fifth order Butterworth filter is shown in Figure 3.2 where the frequency sample point 127 corresponds to the Nyquist or the fold-over frequency. Note that this function is the magnitude squared function of the generally used Butterworth filters.

Standard finite impulse response (FIR) filters can be designed using various techniques and easily applied in our application. One useful, simple way of designing an FIR filter is to use the windowing techniques. Design of a lowpass FIR filter using windowing can easily be carried out as described in [12]. Experiments in Chapter IV use filters designed using a Blackman window. A typical frequency response of the FIR filter obtained using the Blackman window is shown in Figure 3.3 (Nyquist frequency corresponds to the sample point 127 so f_c is again 32).

More sophisticated FIR filters could be obtained by computer aided design and several commercial software packages are available for this purpose. A frequency selective filter with an equiripple approximation can be designed by the software package described in [24]. The filter length and stopband and passband regions are given as inputs and the program turns out the optimal

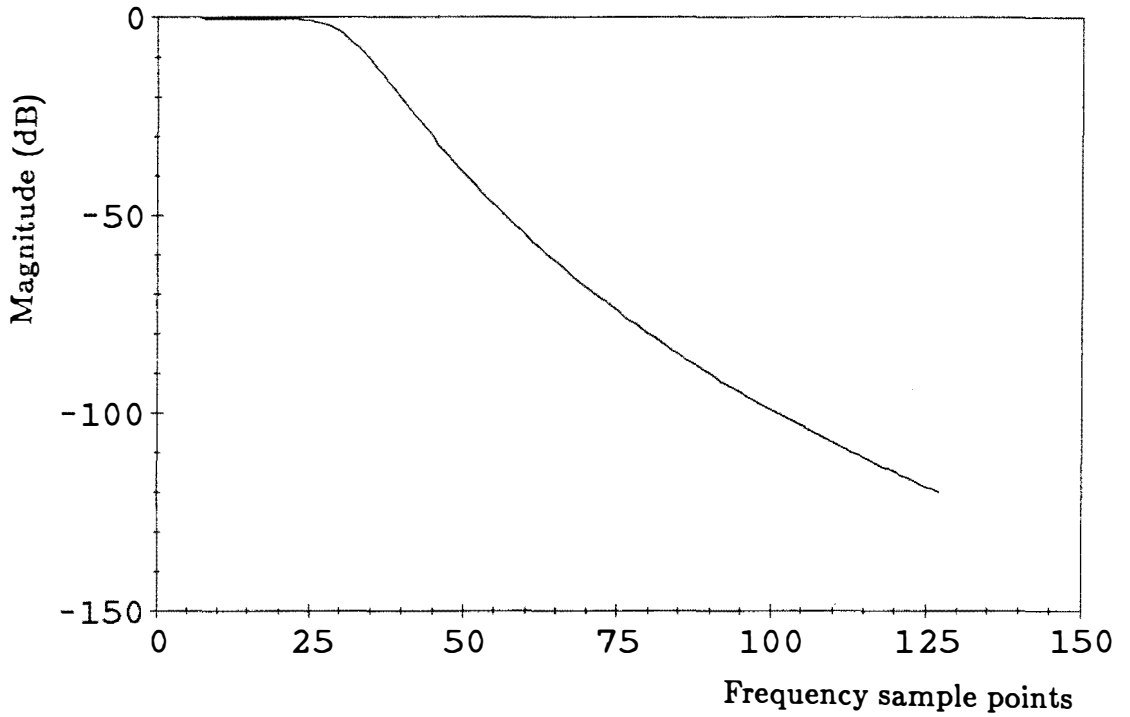

Figure 3.2. Butterworth filter magnitude response (fifth order, $f_c = 32$).

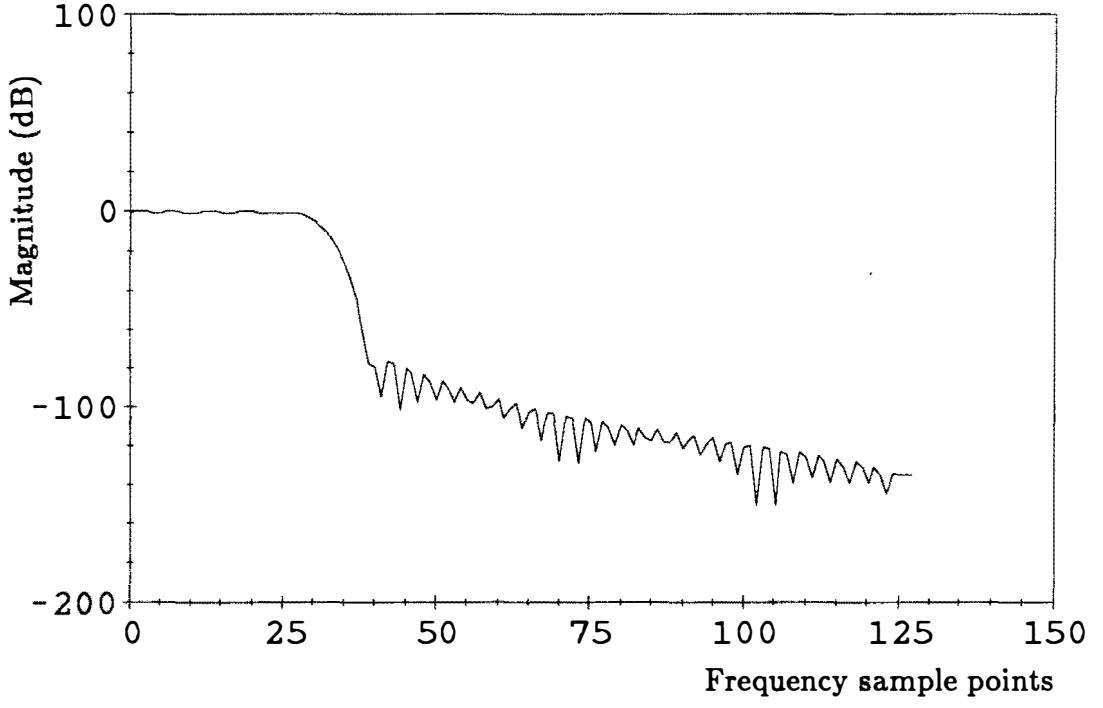

Figure 3.3. FIR Blackman windowed filter magnitude response (passband edge frequency = 0.125, filter length = 43).

impulse response for the desired filter. The term "optimal" is used as the frequency samples are adjusted to improve the filter frequency response by minimizing the maximum deviation between the filter frequency response and the desired frequency response. The optimization uses linear programming techniques, specifically a procedure known as the Remez exchange algorithm, and the resulting frequency response has equal ripples of uniform amplitude in the passband and stopband. The design with a narrower transition-band will consume more computational time and will not produce better stopband attenuation as in the case of a wide transition-band design. A typical frequency response of the optimal filter used in our applications is shown in Figure 3.4. This filter has a passband between 0.0 and 0.115 and a stopband between 0.135 and 0.5, where the frequencies are specified in terms of the fraction of the sampling frequency. The filter length was selected to be 43.

Optimal filters are generally preferred over the other filters mentioned above. Most of the experiments carried out in Chapter IV use the optimal filters. The Butterworth filter and the FIR filter designed using the Blackman window are easily obtainable and some other experiments in Chapter IV show the applicability of those filters. Zero-padding was employed with all the FIR filters to guarantee that there would be no undesirable circular convolution effects.

Once the filtered DFT is obtained the DFT of the symmetrized data need to be calculated to proceed with the Hankel transform computation to obtain $\hat{\epsilon}(l)$.

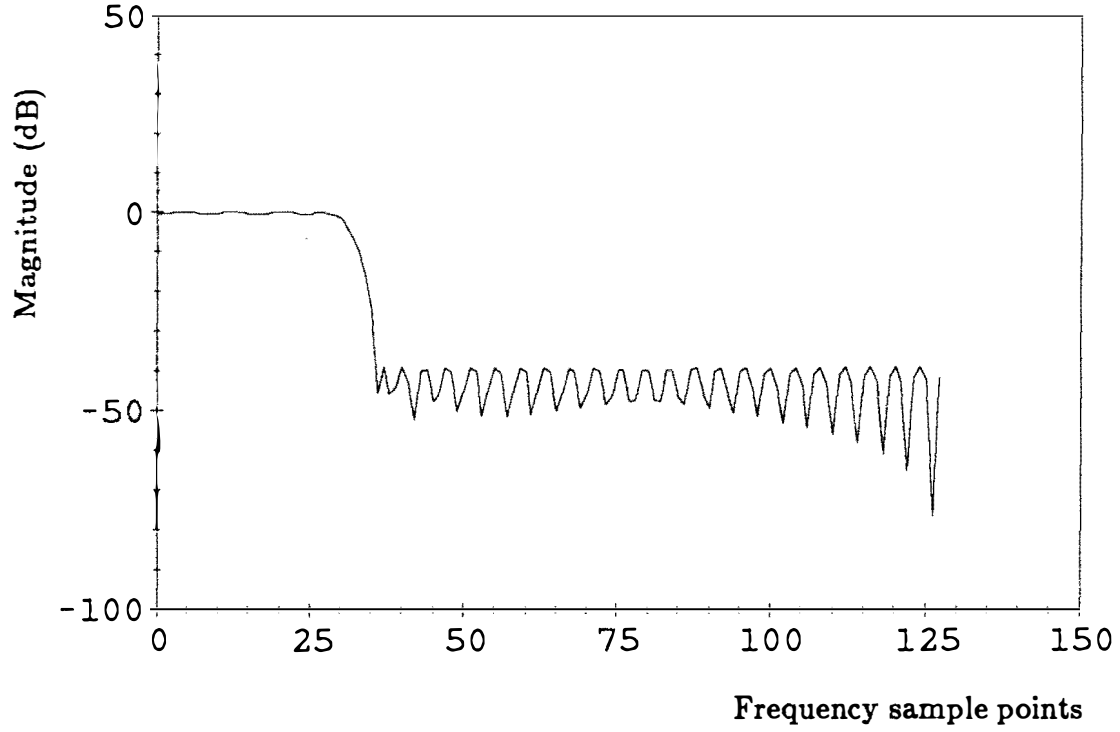

Figure 3.4. FIR optimal filter magnitude response.

The estimation of the shift of the intensity profile from the geometrical center is carried out after the lowpass filtering to avoid any effect on the estimate by unsymmetrical high frequency components. Some important properties of the DFT can be used along with assumed noise characteristics to estimate the shift of the input intensity profile from the geometrical center [25]. As stated earlier, the input data is shifted and corrupted with noise. Therefore, an input sequence obtained from the actual observed intensity image can be written as,

$$\hat{I}_n(i) = \hat{I}(i + \Delta i) + \hat{\eta}(i) \quad ; \quad i = 0,1,...,N-1 \tag{3.2}$$

where Δi is the unknown shift and $\hat{\eta}(i)$ is the sequence corresponding to the noise. It is now required to extract the sequence $\hat{I}(i)$ from $\hat{I}_n(i)$. The DFT of this sequence is [12],

$$\hat{G}_n(k) = \hat{G}(k)e^{j\frac{2\pi k\Delta i}{N}} + \hat{N}(k) \tag{3.3}$$

where $\hat{N}(k)$ is the DFT of the noise sequence and Equation **3.3** is written using the DFT shift theorem which can be shown to be valid for non-integer values of Δi also (see Appendix A) [25]. The required information $\hat{I}(i)$ is real and symmetric (even) and so is the DFT $\hat{G}(k)$. Therefore, the imaginary part of the DFT of the properly centered data should totally correspond to the noise. If the real and imaginary parts of $\hat{G}_n(k)$ are given by $\hat{G}_R(k)$ and $\hat{G}_I(k)$ and those of

$\hat{\mathcal{N}}(k)$ are given by $\hat{\mathcal{N}}_R(k)$ and $\hat{\mathcal{N}}_I(k)$, then

$$\hat{\mathcal{N}}_I(k) = \hat{G}_I(k)\cos(2\pi k\Delta i/N) - \hat{G}_R(k)\sin(2\pi k\Delta i/N) \quad . \tag{3.4}$$

To obtain this, Equation 3.3 is multiplied by $e^{-j\frac{2\pi k\Delta i}{N}}$. Then, assuming stationary noise, the shift applied to $\hat{\mathcal{N}}_I(k)$ can be ignored and Equation 3.4 results.

Note that the lowpass filtering will not completely eliminate the noise. The noise is assumed to be a zero-mean, Gaussian random process. The imaginary part of the DFT of the noise sequence can be considered to be a linear transformation of $\hat{\eta}(i)$. Then the joint probability function for an ensemble of uncorrelated $\hat{\mathcal{N}}_I(k)$; $k = 0, 1, ..., N/2 - 1$ is written as [26]

$$p(\mathcal{N}_I) = C \prod_{k=0}^{N/2-1} \exp\{\frac{-\hat{\mathcal{N}}_I^2(k)}{\sigma^2}\} \tag{3.5}$$

where C and σ are constants. Then the probability of $\hat{\mathcal{N}}_I(k)$ given the shift Δi can be written using the substitution given by Equation 2.4 as follows:

$$p(\mathcal{N}_I/\Delta i) = C \exp\{-\sum_{k=0}^{N/2-1} [\hat{G}_I(k)\cos(2\pi k\Delta i/N) - \hat{G}_R(k)\sin(2\pi k\Delta i/N)]^2/\sigma^2\} \quad . \tag{3.6}$$

The maximum likelihood estimator can be derived by maximizing this function [25]. Differentiating with respect to Δi results in an expression,

$$\sum_{k=0}^{N/2-1} \{[\hat{G}_R^2(k) - \hat{G}_I^2(k)]\sin\alpha - 2\hat{G}_R(k)\hat{G}_I(k)\cos\alpha\}k = 0 \qquad (3.7)$$

where $\alpha = (4\pi k\Delta i)/N$.

The solution for Δi satisfying Equation 3.7 can not be written explicitly and can be obtained by an iterative technique (see Appendix B). However, to arrive at a quick solution the beginning value for the iterative procedure should be as close as possible to the exact value. A tentative beginning value for Δi can be obtained by considering a noise-free situation. If the input data is noise-free then the phase of the Fourier transform will give the amount of shift as given by Equation 3.3. This value will vary for each discrete sample frequency point in the noisy case and any non-zero value may be suitable for a beginning Δi to the iterative procedure. A range of Δi is first detected so that the summation in Equation 3.7 changes its sign with in the interval. Then the interval is narrowed down by successive approximation to an acceptable small value. The mid-point of that interval is chosen as the best suitable value for Δi. The steps involved in this procedure are given in Appendix B. The experiments in Chapter IV indicate that this technique works very well.

For noise which is not Gaussian the shift determined by the technique above is no longer a maximum likelihood estimator. However, the technique is still effective for determining the shift in that case.

Once the best suitable Δi is found, the DFT shift theorem can be used

to find the DFT of the symmetrized data. A small amount of imaginary part information may still be left. This represents the spectrum of the noise remaining after filtering and is useful in evaluating the accuracy of the inverted result. The Hankel transform of the real part is computed to obtain $\hat{\epsilon}(l)$.

CHAPTER IV

NUMERICAL EXPERIMENTS

Experiments have been carried out in two parts. The first part deals with the noise-free data and mainly compares the accuracy and computational complexity of Abel inversions performed with different Hankel transform routines. A table of Abel transforms for various functions is given by Bracewell [10]. Two functions are selected, properly sampled, and Abel inverted to compare with the tabulated inversions. In the second part of the experiments, the input data is corrupted with generated noise, shifted and inverted to see the effect of filtering and the symmetrizing routine.

Before proceeding to the results of the experiments it is necessary to examine certain details involved in implementing the procedure described in Chapter II. When evaluating the sum in Equation 2.13 the important dc value $\hat{G}(0)$ becomes ineffective as it is multiplied by $k = 0$. The function $G(f)$ is represented by rectangles with base of unit length ($= \Delta f$) and height $\hat{G}(k)$ centred at each k as shown in Figure 4.1. The first rectangle actually has width 0.5 and is centered at $k = 0.25$. Therefore, the value of $k\hat{G}(k)$ corresponding to $k = 0$ can be replaced by $(0.5)(0.25)\hat{G}(0)$ so that the dc value becomes effective. Similar precautions must be taken in performing the FFT in Equation 2.19. In this case $k\hat{G}(k)$ for $k = 0$ can be replaced by $(0.25)\hat{G}(0)$, since $fG(f)$ is taken as an even function.

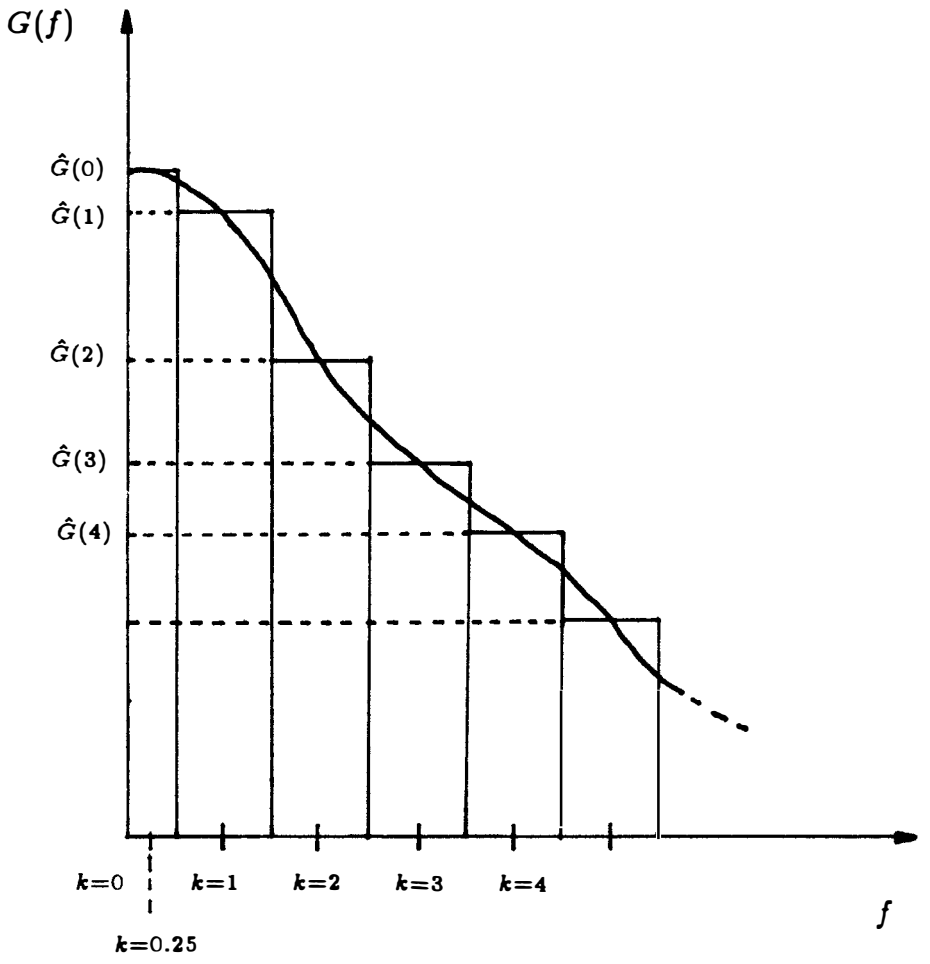

Figure 4.1. Discrete rectangular approximation of a continuous function.

Experiments with Noise-Free Data

The first theoretical data set is a sequence obtained by sampling a Gaussian function defined as follows.

$$\hat{I}_1(i) = e^{-(i/10)^2} \quad ; \quad i = 0, 1, ..., 128 \quad . \tag{4.1a}$$

The Abel inversion of $I_1(i)$ with an even extension in negative i axis is theoretically given by [10],

$$\hat{\epsilon}_1(l) = \frac{1}{10\sqrt{\pi}} e^{-(l/10)^2} \quad ; \quad l = 0, 1, ..., 128 \quad . \tag{4.1b}$$

Figure 4.2 shows the first 64 significant points of $\hat{I}_1(i)$ (only the positive axis is shown since the sequence is symmetric.). The sequences are Abel inverted with the Direct, FSS and MFSS Hankel transform routines. The inversions are plotted with the exact transforms given by Equation 4.1a and shown in Figures 4.3a, 4.3b and 4c. The mean squared error (MSE) values for various inversions are very small. Also, the mean squared error for the inversion with the MFSS Hankel transform routine is comparable with that of the inversions with a Direct or FSS Hankel transform routines. The first significant 64 points are only shown in figures for clarity.

Although most practical functions are similar to the Gaussian function and give nearly perfect inversions, there are certain functions which do not behave

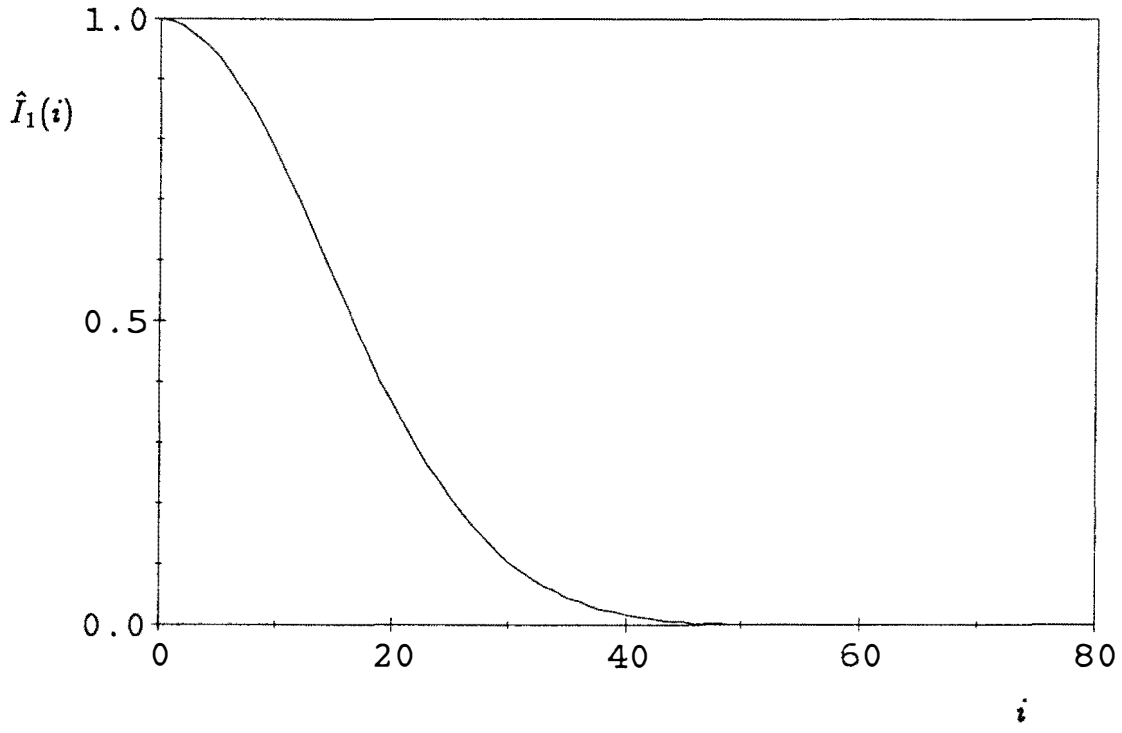

Figure 4.2. Input profile $\hat{I}_1(i)$.

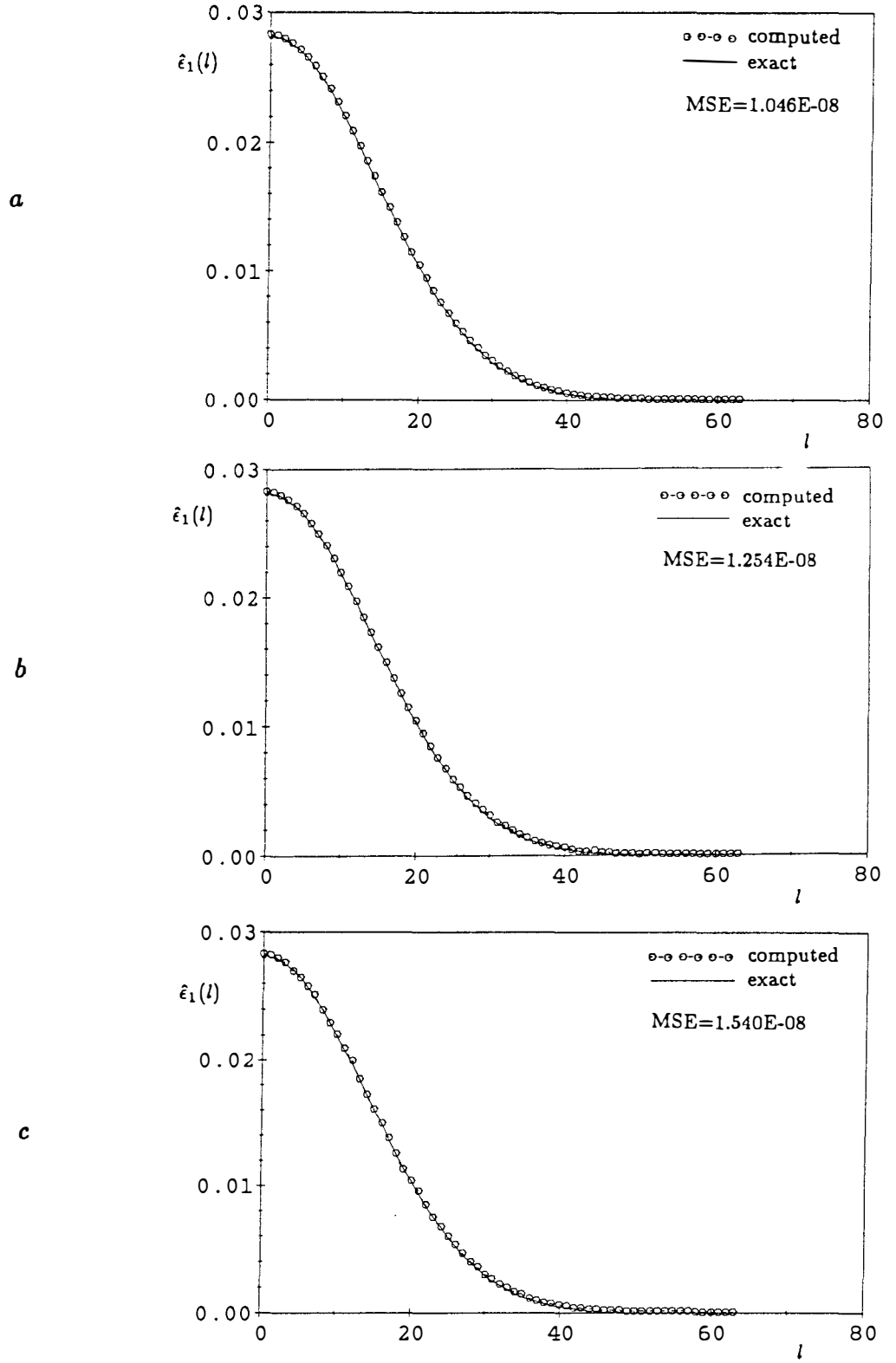

Figure 4.3. Inversion of $\hat{I}_1(i)$. a. Using the Direct Hankel transform routine; b. Using the MFSS Hankel transform routine; c. Using the MFSS Hankel transform routine

well in the numerical procedure. These functions are of less practical importance, but later it is shown that they can be used in determining filter specifications for noisy data. One good example of this kind of function is a semi-ellipse, for which the exact inversion is a pill box function. The pair is defined by,

$$\hat{I}_2(i) = \begin{cases} \frac{1}{40}(40^2 - i^2)^{0.5} & ; \quad i = 0, 1, ..., 40 \\ 0 & ; \quad i = 41, 42, ..., 128 \end{cases} \tag{4.3a}$$

$$\hat{\epsilon}_2(l) = \begin{cases} 0.0125 & ; \quad i = 0, 1, ..., 40 \\ 0 & ; \quad i = 41, 42, ..., 128 \end{cases} . \tag{4.3b}$$

The input data profile $\hat{I}_2(i)$ is shown in Figure 4.4. The results of the experiments are shown in Figures 4.5a, 4.5b and 4.5c. The ripples in the numerical inversion are caused by the well known Gibbs phenomena [12]. The number of terms required to guarantee convergence of the Fourier-Bessel series for the pill box function is large. A higher sampling rate in the intensity domain will give more high frequency information, and this, in turn, may produce a better inversion. It is interesting to note that the error produced by the inversion with a Direct Hankel transform routine is regular, in the sense that the ripple amplitudes gradually increase toward the discontinuity, and also reach the peak at the discontinuity point. Another important observation is that the FSS and the MFSS Hankel transform routines inject random errors which may mainly be due to the nearest neighbor interpolation described in Chapter II. However, the

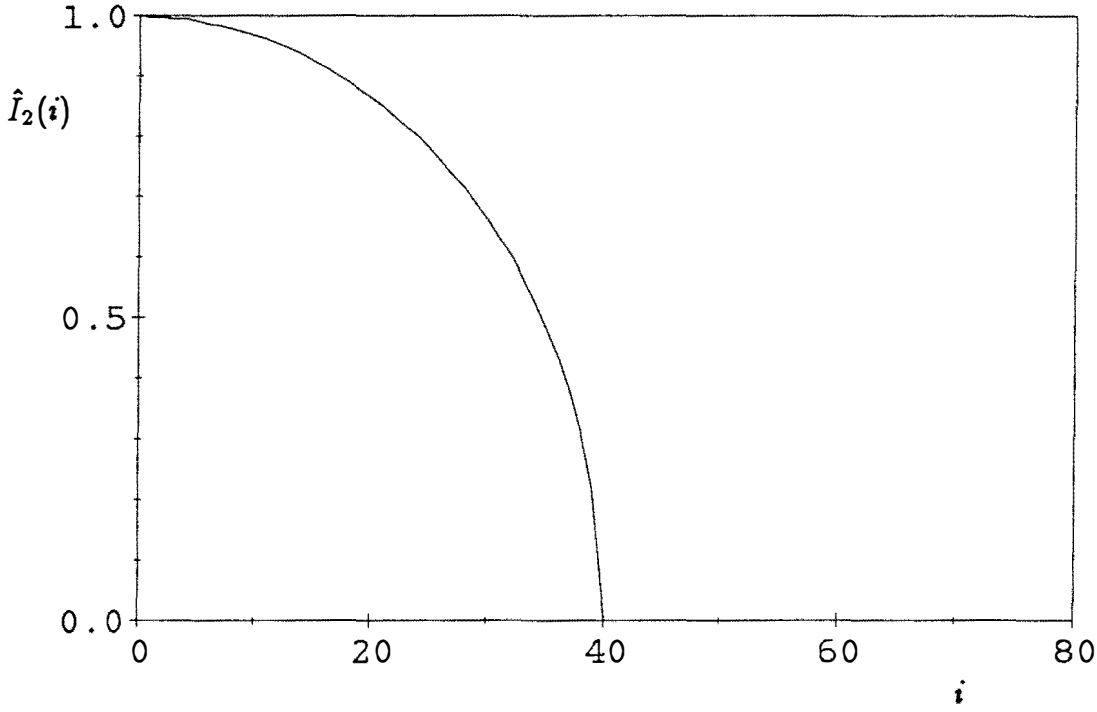

Figure 4.4. Input profile $\hat{I}_2(i)$.

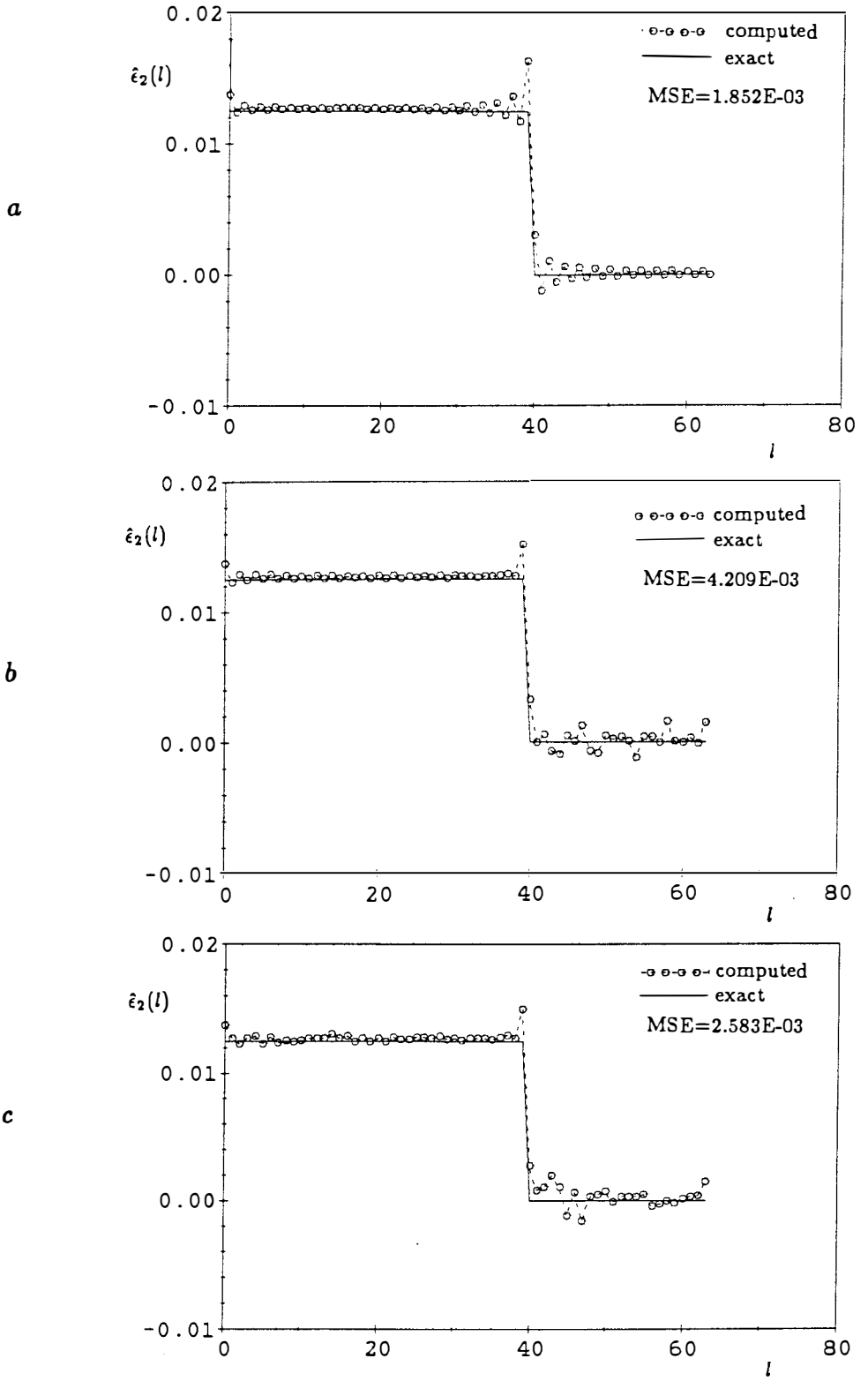

Figure 4.5. Inversion of $\hat{I}_2(i)$. a. Using the Direct Hankel transform routine; b. Using the MFSS Hankel transform routine; c. Using the MFSS Hankel transform routine

lower order components are fairly accurate in the inversions using the FSS and the MFSS algorithms, and this, in turn, suggests that the Dual algorithm [20] may well be suited to perform the Hankel transform in this case.

The mean squared error values of the results of the experiments carried out are summarized in Table 4.1. When the mean squared error values for various experiments and the computational complexity given in Table 2.1 and 2.2 are considered, the MFSS algorithm seems to be a reasonable choice. Practical situations, mostly, require inversions of intensity profiles similar to Gaussian functions and, as we see in the experiments, the MFSS gives good results for those cases. If we use a computer which takes twice the time to multiply as it does to add, a 128-point MFSS Hankel transform routine will be approximately three times faster than the Direct Hankel transform routine.

Table 4.1. Comparison of Abel inversions in terms of accuracy.

	Mean Squared Error (MSE)		
Input	Direct	FSS	MFSS
$\hat{I}_1(i)$	1.046E-08	1.254E-08	1.540E-08
$\hat{I}_2(i)$	1.852E-03	4.209E-03	2.583E-03

Experiments with Noisy Data

The second part of the experiments is to see the behavior of the inversion of noisy data using the filtering and symmetrizing methods described in Chapter III. Experiments require a random noise sequence with a Gaussian probability density function. Two sets of zero mean random numbers are generated and are used to generate another set of random numbers with a Gaussian density function. This procedure is given in detail in [27]. Then, the generated numbers are attenuated to give a random sequence with a desired variance. A random sequence with a variance of 0.001 and a length of 256 was added term by term to the sequence $\hat{I}_1(i)$ and shifted by two integer sample points to produce a new sequence $\hat{I}_{n1}(i)$. Also, the sequence was zero padded so that the filtering by DFT's produce a linear convolution filtering. The generated noisy data profile is shown in Figure 4.6.

Table 4.2. Specifications of the optimal filters used in the experiments.

Filter	Passband	Stopband
Filter 1	0.0 to 0.1150	0.1350 to 0.5
Filter 2	0.0 to 0.0525	0.0725 to 0.5
Filter 3	0.0 to 0.0215	0.0415 to 0.5

Three optimal filters are chosen and their desired frequency characteristics are shown in Table 4.2. The mid-points of the transition-bands are chosen to be 0.125, 0.0625 and 0.03125 for Filter 1, Filter 2 and Filter 3 respectively. Note that the frequency is given in terms of the fraction of the sampling frequency and a passband of 0.0 to 0.5 designates an allpass filter.

The experiments in this part use the MFSS algorithm to compute the Hankel transform. First $\hat{I}_{n1}(i)$ is inverted without filtering or symmetrizing and the outcome is shown in Figure 4.7. Then the inversion incorporating the filtering and symmetrizing procedures was performed on the data with Filter 1 and the result is shown in Figure 4.8. Figures 4.9 and 4.10 show the inverted data profiles which used Filter 2 and Filter 3 respectively. The inversion with Filter 1 does not reduce much of the noise and the inversion with Filter 2, which has narrower passband bandwidth, gives better results. However, when the bandwidth is further reduced (Filter 3) the attenuation of the desired information occurs. The distortion can be observed in Figure 4.10. Filter 2 appears to be the most suitable filter for the inversion of the theoretical data set, $\hat{I}_{n1}(i)$.

The optimal filters are not always easily designed and are usually obtained using commercially available software packages. To show the applicability of the easily designed filters, two other lowpass filters, namely the Butterworth filter (fifth order, $f_c = 16$) as described in Chapter III and a Blackman windowed FIR filter of bandwidth 0.0625 are applied and the results are shown in Figures 11a

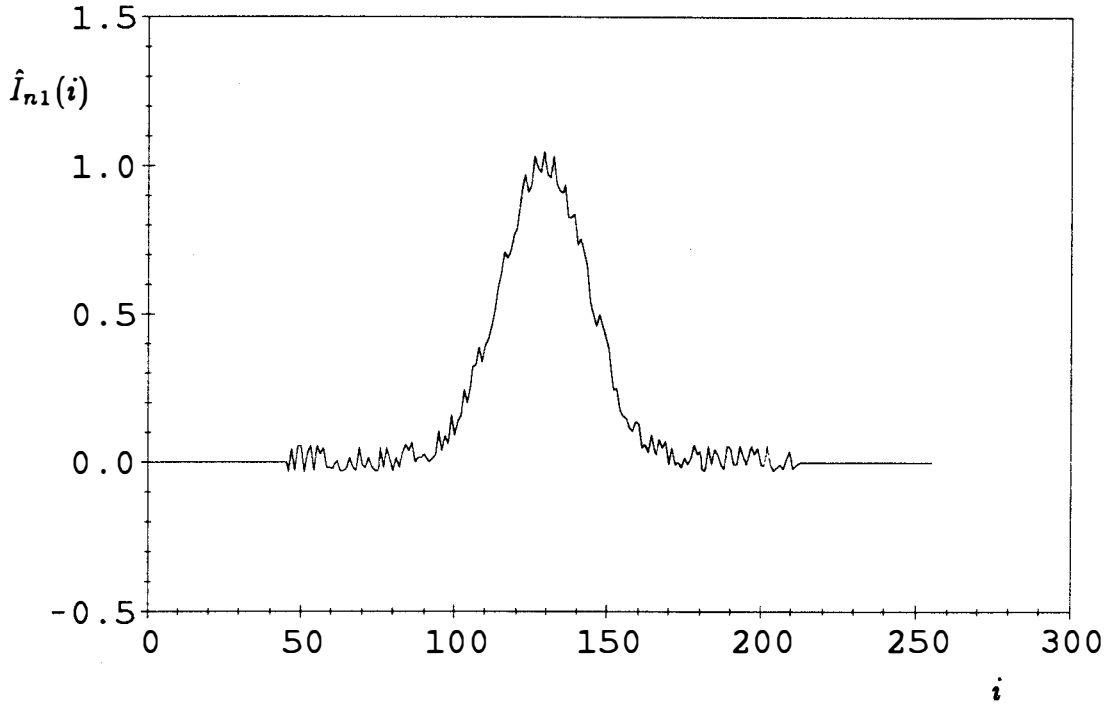

Figure 4.6. Generated noisy data $\hat{I}_{n1}(i)$.

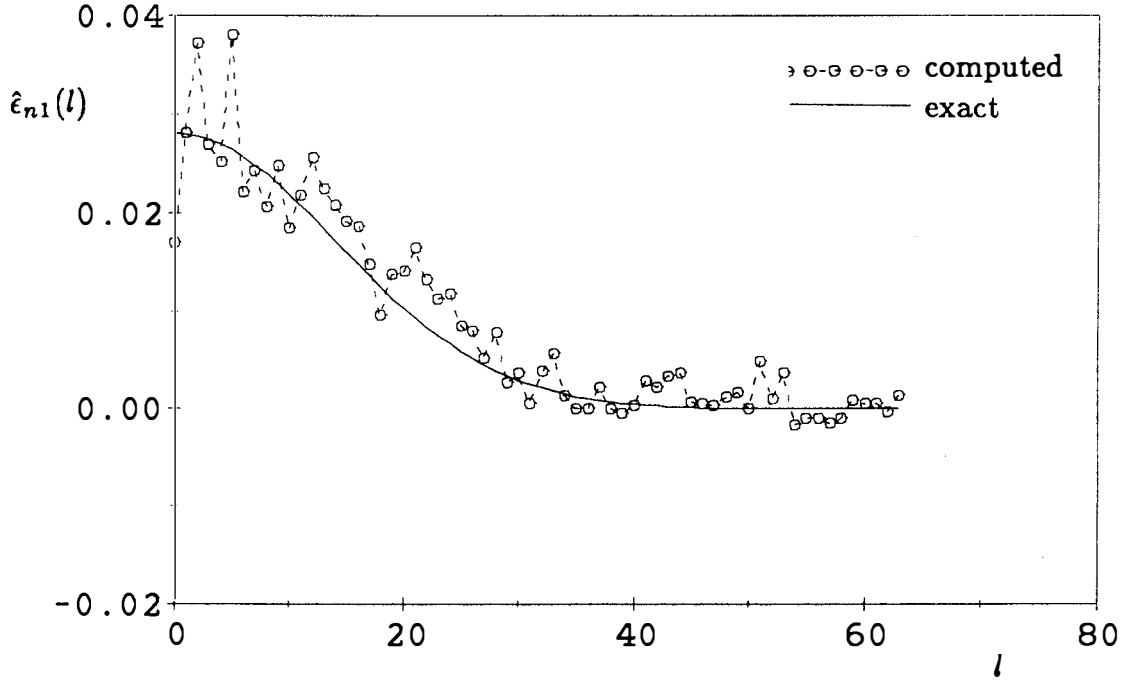

Figure 4.7. Inversion of $\hat{I}_{n1}(i)$ without filtering or symmetrizing.

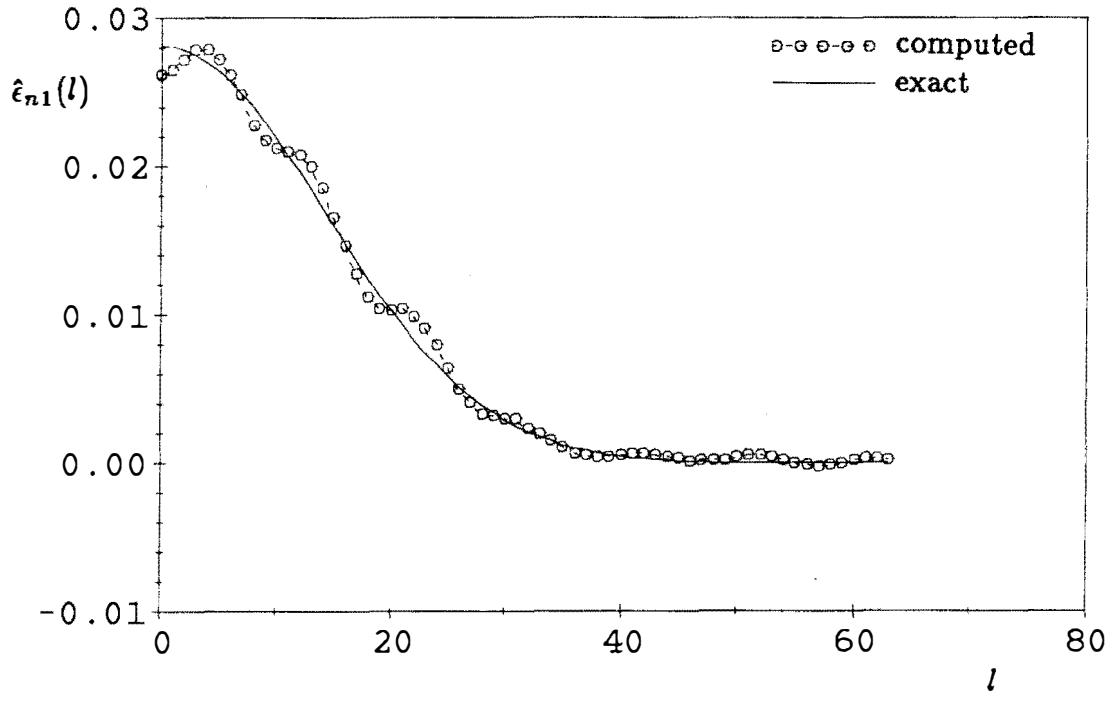

Figure 4.8. Inversion of $\hat{I}_{n1}(i)$ using Filter 1.

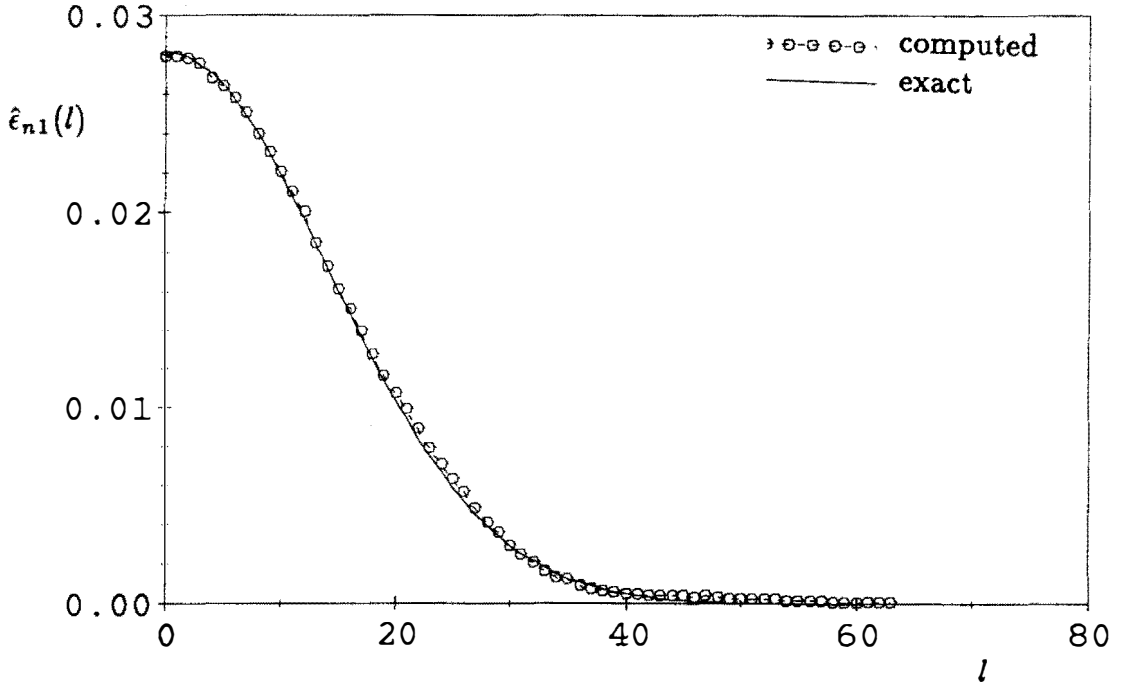

Figure 4.9. Inversion of $\hat{I}_{n1}(i)$ using Filter 2.

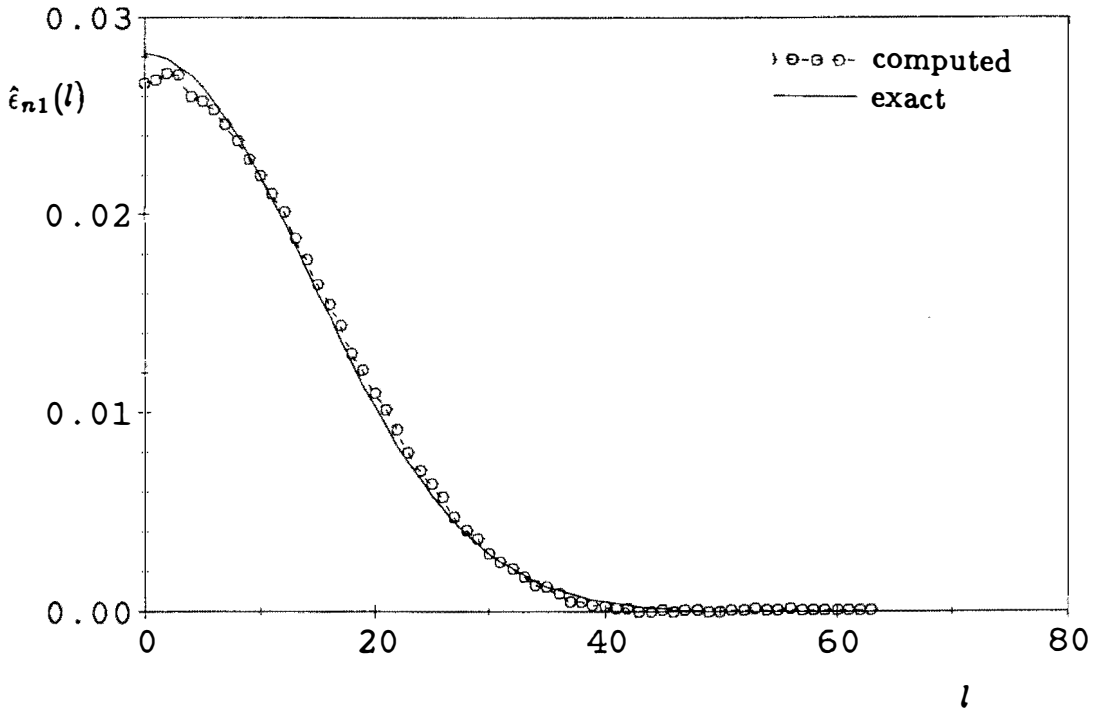

Figure 4.10. Inversion of $\hat{I}_{n1}$ using Filter 3.

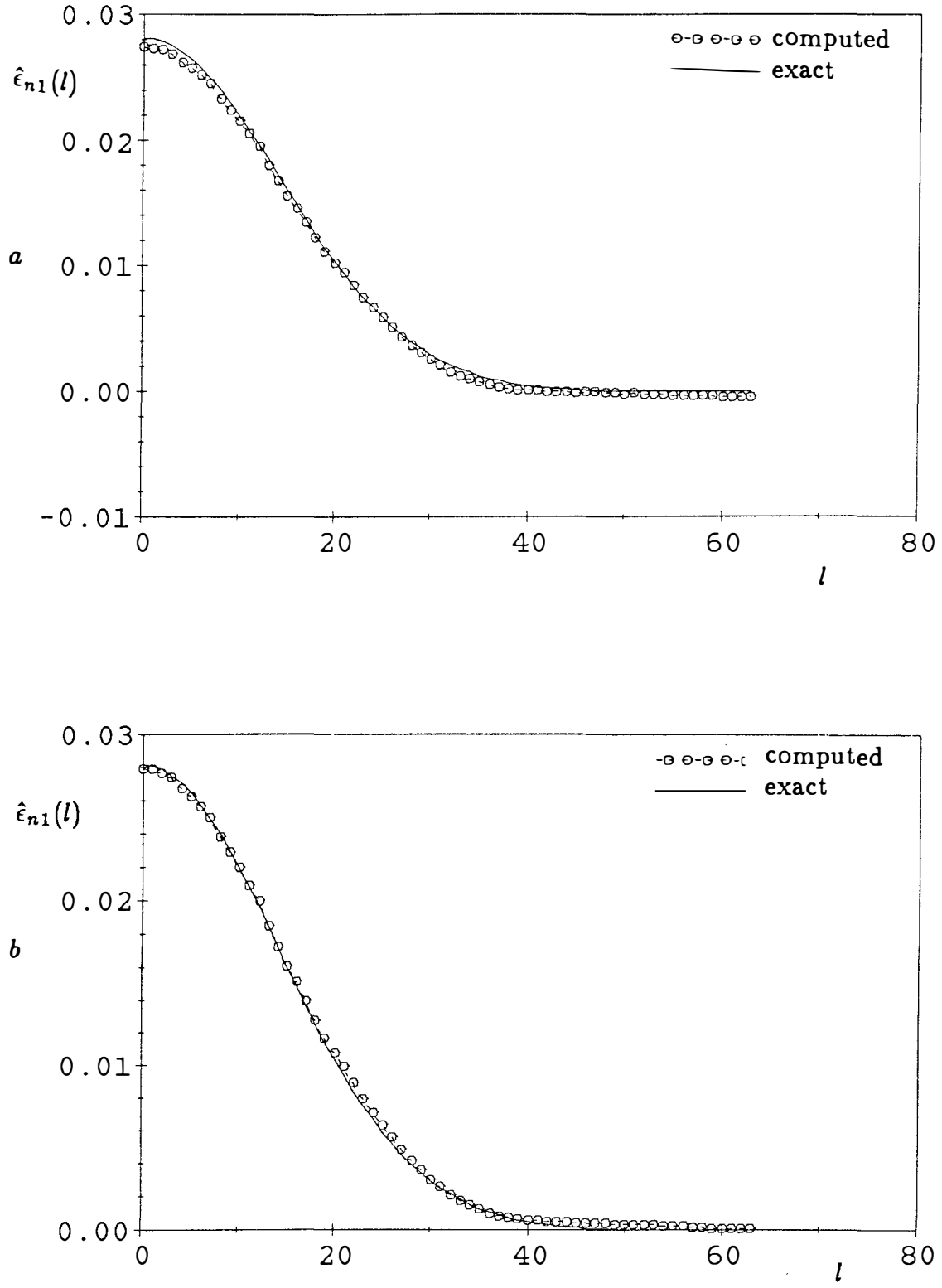

Figure 4.11. Inversion of $\hat{I}_{n1}(i)$. a. Using Butterworth filter; b. Using Blackman windowed FIR filter

and 11b. Note that the Butterworth filter is applied to the data set which is not zero-padded. The optimal filter performs slightly better than both these filters (Figure 4.8). However, the differences are small and the Butterworth filter has an advantage of processing the data without zero-padding. The availability of filter design software, the computational speed, required accuracy and the above results can be combined to select a proper filter for actual data.

The sequence $\hat{I}_{n1}(i)$ had most of its energy in the low frequency range and the application of a narrow passband lowpass filter was possible (Filter 2). However, the following experiments show the difficulties encountered in selecting the bandwidth for certain kind of input sequences.

The sequence $\hat{I}_2(i)$ and the generated noise sequence are added term by term to generate another set of noisy data $\hat{I}_{n2}(i)$. The generated noisy data profile, $\hat{I}_{n2}(i)$, is shown in Figure 4.12. The inversions shown in Figures 4.13, 4.14 and 4.15 are obtained using Filter 1, Filter 2 and Filter 3 respectively. Filter 1 does not reduce the noise to a satisfactory level. Also, the effect of Gibbs phenomena is more pronounced due to the removal of the high frequency information. Although the filters with narrower passband bandwidth (Filter 2 and Filter 3) reduce the noise, the output clearly is distorted. This inversion exemplifies the trade-offs in selecting filter bandwidth. Filter 1 seems preferable in this case because the distortion is not desirable in most cases. Fortunately, sequences like $\hat{I}_2(i)$ are rare in reality.

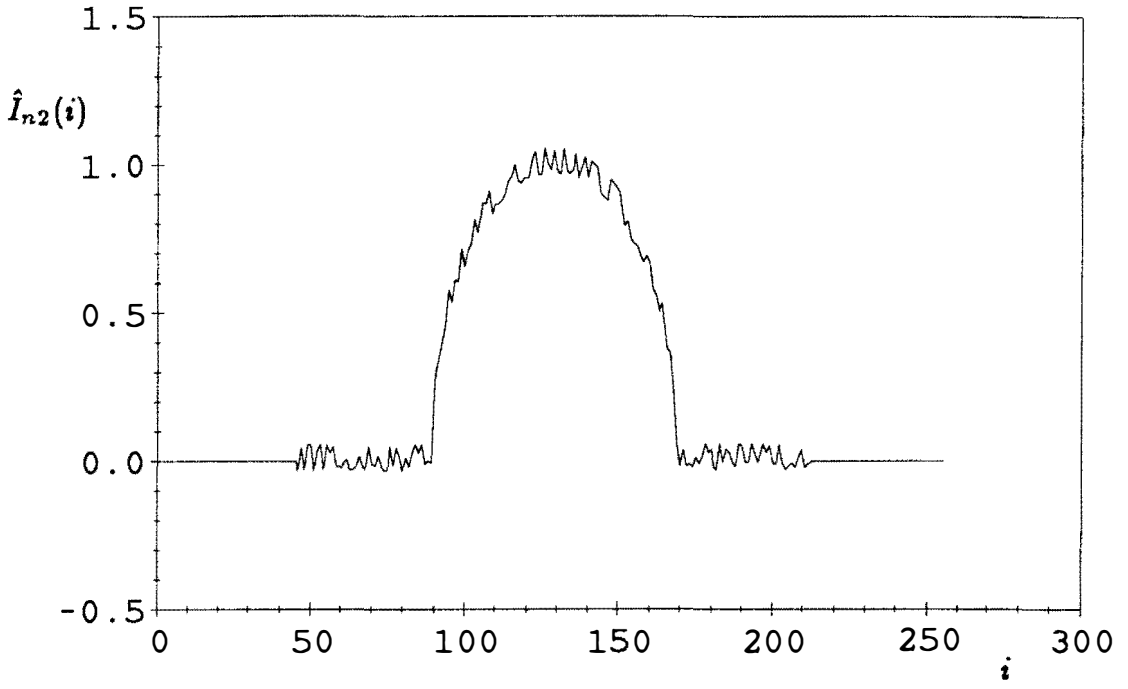

Figure 4.12. Generated noisy data $\hat{I}_{n2}(i)$.

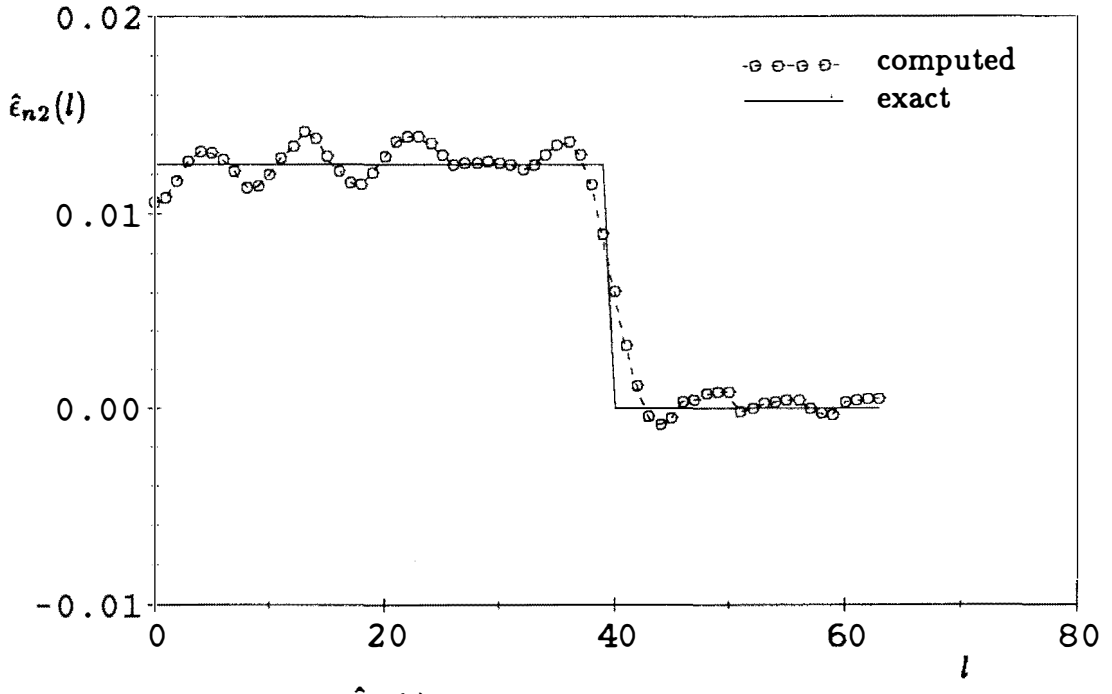

Figure 4.13. Inversion of $\hat{I}_{n2}(i)$ using Filter 1.

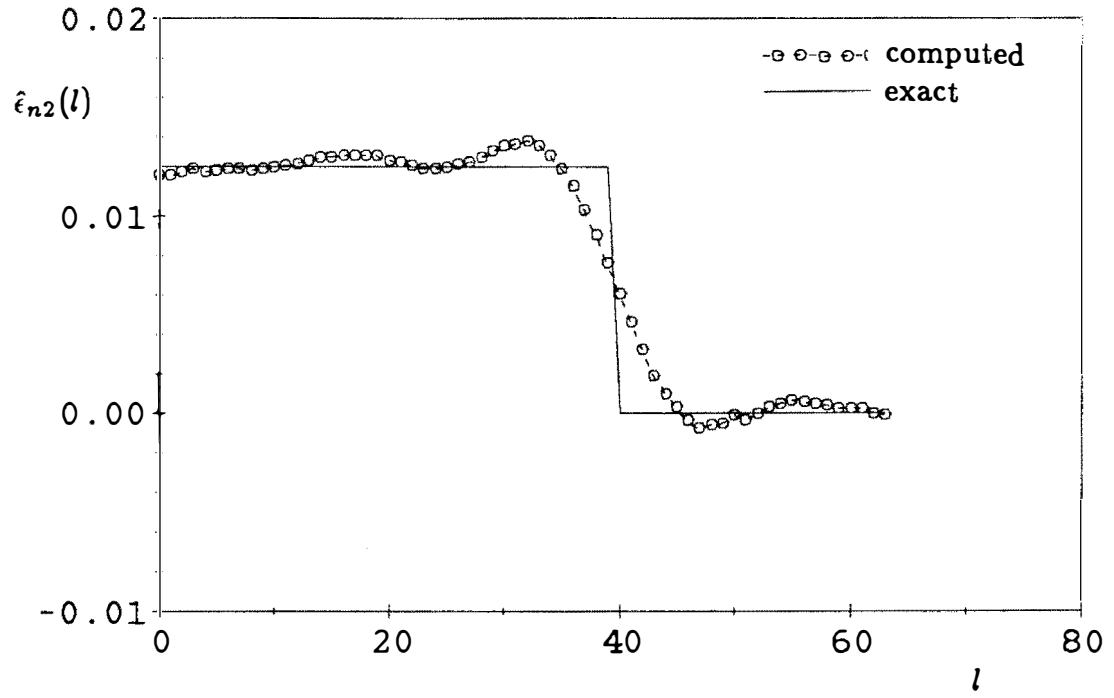

Figure 4.14. Inversion of $\hat{I}_{n2}(i)$ using Filter 2.

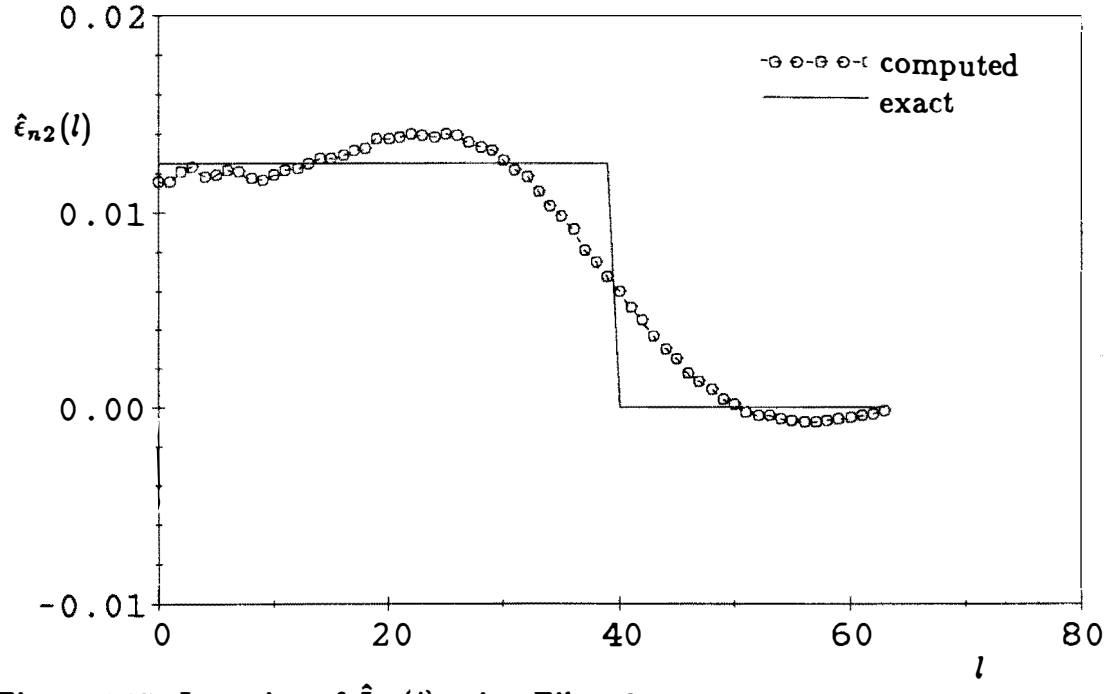

Figure 4.15. Inversion of $\hat{I}_{n2}(i)$ using Filter 3.

CHAPTER V

SUMMARY AND CONCLUSIONS

A new method has been developed for the Abel inversion of measured intensity data in the presence of noise. The Abel inversion or the inverse Abel transform is performed by the Fourier transform followed by the inverse Hankel transform. The efficiency of the well known FFT is exploited in the evaluation of both the Fourier and inverse Hankel transforms. The experimental intensity data is usually noisy and off-center. This fast technique is made applicable to noisy data by frequency domain filtering and a maximum likelihood estimator derived from the assumed noise characteristics. Results of several numerical experiments have been presented to determine filter specifications for practical data.

The proposed method has a number of advantages over the existing curve-fit techniques. Curve-fitting methods neither considered the spectral characteristics of the noise and the desired information, nor addressed the problem of symmetrizing as clearly as described in Chapter III.

The principal advantage of the proposed method is its computational efficiency. For instance, the inversion of 512 sets of 240-point data consumed about eight minutes of CPU time when processed by this method in contrast to a 20 hour CPU time required for a curve-fit inversion using the method described in [7]. The data analysis was carried out in a Masscomp MC500

Micro Supercomputer. The symmetrizing procedure generally consumed about five to seven iterations for each set of data. Contour plots of the intensity and the emission coefficient images are given in Figure 5.1 and Figure 5.2. If the data analysis program is implemented in faster computers incorporating data acquisition systems, the Abel inverted images may be obtained on-line from digitized intensity images.

Further research should be carried out to extend this method to perform asymmetrical Abel inversions since asymmetrical inversions are also of interest to the experimentalists [8]. Recently a method described by Hansen and Law [28] was introduced which claims to be more efficient than the curve-fit techniques. In [28], the inverse Abel transform integral is approximated by a state variable model to compute the inversion recursively and the noise is handled by space domain Kalman filtering. However the symmetrizing problem is not addressed and a first hand look at the computational complexity suggests that the integral transform approach may be more efficient. The accuracy and the computational efficiency of these two techniques should be compared in future research.

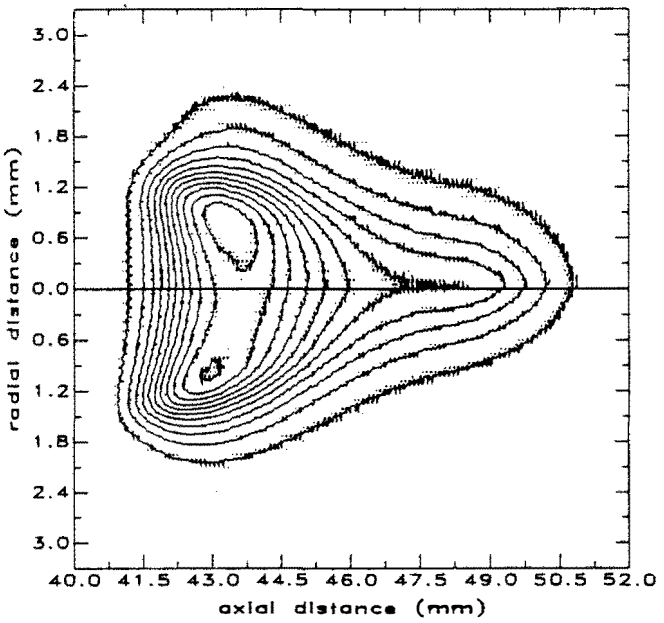

Figure 5.1. Contour plot of the intensity image.

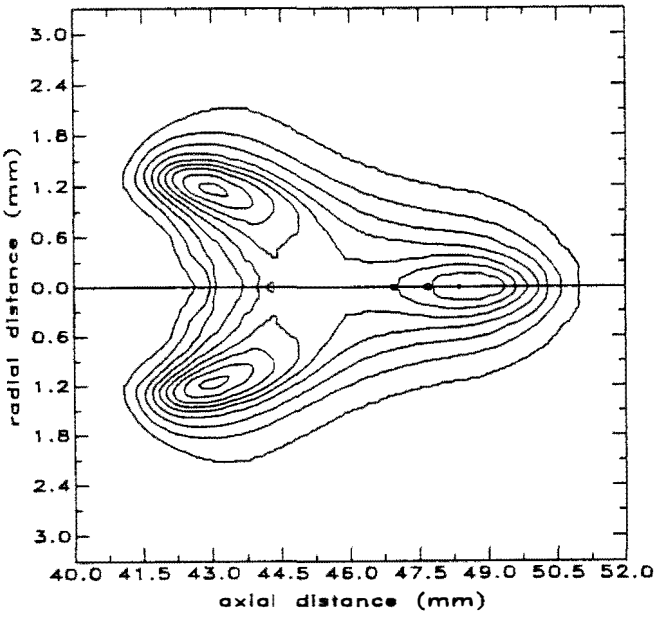

Figure 5.2. Contour plot of the emission coefficient image.

BIBLIOGRAPHY

BIBLIOGRAPHY

1. H. R. Griem, Plasma Spectroscopy, McGraw-Hill, New York, 1964.

2. R. N. Bracewell, The Fourier Transform and Its Applications, McGraw-Hill, New York, 1965.

3. O. H. Nestor, and H. N. Olsen, "Numerical Methods for Reducing Line and Surface Probe Data," SIAM Review 2, pp 200-207, 1960.

4. K. Bockasten, "Transformation of Observed Radiances into Radial Distribution of the Emission of a Plasma," Journal of the Optical Society of America, 51(No. 9), pp 943-947, 1961.

5. M. J. Freeman and S. Katz, "Determination of A Radiance Coefficient Profile from the Observed Axisymmetric Radiance Distribution of an Optically Thin Radiating Medium," Journal of the Optical Society of America, 53(No. 10), pp 1172-1174, 1963.

6. C. J. Cremers and R. C. Birkebak, "Application of the Abel Integral Equation to Spectrographic Data," Applied Optics, Volume 5, No. 6, 1966.

7. R. T. Shelby, Unpublished Master's Thesis, The University of Tennessee, Knoxville, Tennessee, 1976.

8. C. D. Maldonado, A. P. Caron and H. N. Olsen, "New Method for Obtaining Emission Coefficients from Emitted Spectral Intensities. Part I - Circularly Symmetric Light Sources," Journal of the Optical Society of America, 55, pp 1247-1254, 1965.

9. R. M. Mersereau and A. V. Oppenheim, "Digital Reconstruction of Multidimensional Signals from Their Projections," Proceedings of the IEEE, Volume 62, No 10, pp 1319-1338, 1974.

10. M. Abramovitz and I. A. Stegun, Handbook of Mathematical Functions, Dover, New York, 1969.

11. A. Antoniou, Digital Filters: Analysis and Design, McGraw-Hill, New York, 1979.

12. A. V. Oppenheim and R. W. Schafer, Digital Signal Processing, Prentice-

Hall, Englewood Cliffs, New Jersey, 1975.

13. J. Brunol and P. Chavel, "Fourier Transformation of Rotationally Invariant Two-Variable Functions; Computer Implementation of Hankel Transform," Proceedings of the IEEE, Volume 65, pp 1089- 1090, 1977.

14. A. V. Oppenheim, G. V. Frisk and D. R. Martinez, "An Algorithm for the Numerical Evaluation of the Hankel transform," Proceedings of the IEEE, Volume 66, pp 264-265, 1978.

15. A. E. Siegman, "Quasi-fast Hankel Transform," Optics Letters, volume 1, pp 13-15, 1974.

16. D. R. Mook, "An Algorithm for the Numerical Evaluation of the Hankel and Abel Transforms," IEEE Transactions on Acoustics, Speech, and Signal Processing, Volume ASSP 31, No. 4, pp 975-985, 1983.

17. P. K. Murphy and N. C. Gallagher, "Fast Algorithms for the Computation of the Zero-Order Hankel Transform," Journal of the Optical Society of America, Volume 73, No. 9, pp 1130-1137, 1983.

18. S. M. Candel, "An Algorithm for the Fourier-Bessel Transform," Computer Physics Communications, Volume 23, pp 343-353, 1981.

19. I. S. Gradshteyn, I.M. Ryzhik, Tables of Integrals, Series and Products, pp 953, Academic Press, New York, 1980.

20. S. M. Candel, "Dual Algorithms for the Fast Calculation of the Fourier-Bessel Transforms," IEEE Transactions on Acoustics, Speech, and Signal Processing, Volume ASSP 29, pp 963- 972, 1981.

21. R. Welle, D. R. Keefer, and C. Peters, "Energy Conversion Efficiency in High-Flow Laser Sustained Argon Plasmas," AIAA paper No. 86-1077, Atlanta, Georgia, May 1986.

22. L. M. Smith, "Non-stationary Noise Effects in the Abel Inversion," to be published in IEEE Transactions on Information Theory, 1986.

23. R. C. Gonzalez, and P. Wintz, Digital Image Processing, Addison-Wesley Publishing Company, Reading, Massachusettes, 1977.

24. Digital Signal Processing Committee, Programs for Digital Signal

Processing, IEEE Press, New York, 1979.

25. L. M. Smith, Private Communication, The University of Tennessee Space Institute, Tullahoma, Tennessee, 1986.

26. E. Parzen, Stochastic Processes, Holden-Day Inc., San Francisco, 1962.

27. D. E. Knuth, The Art of Computer Programming, Volume 2: Semi-Numerical Algorithms, Addison-Wesley Publishing Company, 1971.

28. E. W. Hansen and P. L. Law, "Recursive Methods for Computing Abel Transform and Its Inverse," Journal of the Optical Society of America, Volume 2, No.4, pp 510-520, 1985.

APPENDIXES

APPENDIX A

DFT SHIFT THEOREM FOR NON-INTEGER SHIFTS

Consider a periodic, bandlimited function $x(t)$ with a period t_p so that $x(t) = x(t + it_p)$. If the function is sampled at N points with a sampling interval $T = t_p/N$, then $x(nT)$ can be expressed by a complex Fourier series.

$$x(nT) = \frac{1}{N} \sum_{m=0}^{N-1} C_m \, e^{j \frac{2\pi mnT}{t_p}} \quad ; \quad n = 0, 1, ..., N-1$$

$$\hat{x}(n) = \frac{1}{N} \sum_{m=0}^{N-1} C_m \, e^{j \frac{2\pi mn}{N}} \quad ; \quad n = 0, 1, ..., N-1$$

which is the discrete Fourier series of $\hat{x}(n) = x(nT)$ as given in [12].

Suppose $x_s(t)$ is obtained by shifting $x(t)$ so that $x_s(t) = x(t + \Delta t)$. If $x_s(t)$ is sampled in the same manner as for $x(t)$, $x_s(nT)$ also can be expressed by a Fourier series as

$$x_s(nT) = \frac{1}{N} \sum_{m=0}^{N-1} C_m \, e^{j \frac{2\pi m(n+\Delta n)}{N}} \quad ; \quad n = 0, 1, ..., N-1$$

where $\Delta n = \Delta t/T$. The DFT of $x_s(nT)$, $\hat{X}_s(k)$, is given by,

$$\hat{X}_s(k) = \sum_{n=0}^{N-1} x_s(nT) e^{-j \frac{2\pi kn}{N}} \quad ; \quad k = 0, 1, ..., N-1 \quad .$$

Using the discrete Fourier series,

$$\hat{X}_s(k) = \sum_{n=0}^{N-1} \{ \frac{1}{N} \sum_{m=0}^{N-1} C_m \; e^{j \frac{2\pi m(n+\Delta n)}{N}} \} e^{-j \frac{2\pi k n}{N}}$$

$$\hat{X}_s(k) = \sum_{n=0}^{N-1} \{ \frac{1}{N} \sum_{m=0}^{N-1} e^{j \frac{2\pi n(m-k)}{N}} \; C_m \} \; e^{j \frac{2\pi m \Delta n}{N}} \quad .$$

From [12],

$$\frac{1}{N} \sum_{n=0}^{N-1} e^{j \frac{2\pi n(m-k)}{N}} = \begin{cases} 1 & ; \quad m = k \\ 0 & ; \quad m \neq k \end{cases} \quad .$$

So,

$$\hat{X}_s(k) = C_k \; e^{j \frac{2\pi k \Delta n}{N}} \quad .$$

In [12], it is shown that the Fourier series coefficients C_k are nothing but the DFT of $x(nT)$, $\hat{X}(k)$, at each discrete frequency point k. Hence, the DFT shift theorem,

$$\hat{X}_s(k) = \hat{X}(k) e^{j \frac{2\pi k \Delta n}{N}} \quad .$$

APPENDIX B

ITERATIVE PROCEDURE TO FIND THE SHIFT

1. Compute the DFT, $\hat{G}_R(k) + j\hat{G}_I(k)$, of the input sequence $\hat{I}(i)$.

2. Find $\alpha = \tan(\hat{G}_I(2)/\hat{G}_R(2))$.

3. Set $t_1 = \alpha$; $t_2 = \alpha$; $t_3 = \alpha$.

4. Set $t_1 = t_1 - 0.5$; $t_3 = t_3 + 0.5$.

5. Compute

$$S_1 = \sum_{k=0}^{N-1} \{[\hat{G}_R^2(k) - \hat{G}_I^2(k)]\sin(2t_1k) - 2\hat{G}_R^2(k)\hat{G}_I^2(k)\cos(2t_1k)\}k$$

$$S_3 = \sum_{k=0}^{N-1} \{[\hat{G}_R^2(k) - \hat{G}_I^2(k)]\sin(2t_3k) - 2\hat{G}_R^2(k)\hat{G}_I^2(k)\cos(2t_3k)\}k$$

$$sign = S_1 \times S_3 \quad .$$

6. If $sign > 0.0$ then go to step 4.

7. Compute

$$S_2 = \sum_{k=0}^{N-1} \{[\hat{G}_R^2(k) - \hat{G}_I^2(k)]\sin(2t_2k) - 2\hat{G}_R^2(k)\hat{G}_I^2(k)\cos(2t_2k)\}k$$

$$sign = S_1 \times S_2 \quad .$$

8. If $sign > 0.0$ then go to step 10.

9. Set $t_3 = t_2$; go to step 11.

10. Set $t_1 = t_2$.

11. Set $t_2 = (t_1 + t_3)/2$; $\delta = t_3 - t1$.

12. If $\delta > 10^{-4}$ then go to step 7.

13. Shift = $\Delta i = \frac{Nt_2}{2\pi}$.

VITA

Subramania I. Sudharsanan was born in Dickoya, Sri Lanka on October 17, 1961. He attended elementary and high schools in Jaffna, Sri Lanka. He attended the University of Peradeniya, Sri Lanka, from September 1979 to December 1983, graduating with a Bachelor of Science degree in Electrical and Electronic Engineering.

After working for the Department of Electrical and Electronic Engineering, University of Peradeniya as an instructor, and the Lanka Cement Limited as an instrumentation engineer, he joined the University of Tennessee Space Institute in June 1985. He received a Master of Science degree in Electrical Engineering in August 1986.